Desalination 502 (2021) 114939

Contents lists available at ScienceDirect

Desalination

journal homepage: www.elsevier.com/locate/desal

A review on the synthesis of fully aromatic polyamide reverse osmosis membranes

Shahriar Habib, Steven T. Weinman *

Department of Chemical and Biological Engineering, The University of Alabama, Tuscaloosa, AL 35487, USA

HIGHLIGHTS

- RO membrane synthesis has numerous, important steps.
- RO membrane desalination performance can be tuned by altering synthesis conditions.
- There are numerous ways to synthesize RO membranes.
- Non-reactive additives generally improve desalination performance.
- RO membrane characterization is starting to probe the nano- and Angstrom-scales.

GRAPHICAL ABSTRACT

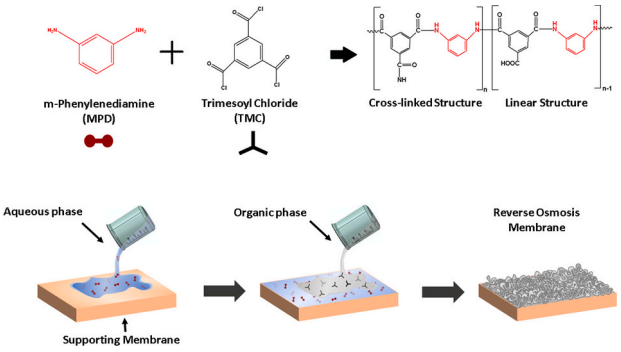

ARTICLE INFO

Keywords:
Thin-film composite membrane
Interfacial polymerization
Desalination
Kinetics
Characterization
Mechanism

ABSTRACT

Reverse osmosis (RO) membranes have been used for desalination for over 40 years. This review focuses on the lab-scale synthesis of fully aromatic polyamide layers used to create RO membranes using the interfacial polymerization (IP) process between an amine monomer, m-phenylenediamine (MPD), and an acyl chloride monomer, trimesoyl chloride (TMC). This review extensively covers the numerous lab-scale synthesis protocols used in research labs and proposed mechanisms and kinetics for synthesizing these fully aromatic polyamide layers using IP. Emphasis is placed on the support membrane used and the reaction conditions such as monomer concentration, solution volume, aqueous solution soaking time, reaction time, reaction temperature, and the use of non-reactive additives in the reaction solution. The effect of processing techniques for removing the aqueous solution and for post-reaction cross-linking are discussed. These variables are compared by investigating their effect on the membrane desalination performance. The numerous methods used to characterize the polyamide layers are reviewed. The synthesis of fully aromatic polyamide layers on hollow fiber membranes is briefly discussed. The goal of this review is to discuss the numerous synthesis parameters in reported lab-scale studies for control membranes, which may help researchers to synthesize and improve RO membranes more effectively.

* Corresponding author.
E-mail address: stweinman@eng.ua.edu (S.T. Weinman).

https://doi.org/10.1016/j.desal.2021.114939
Received 12 August 2020; Received in revised form 15 November 2020; Accepted 25 December 2020

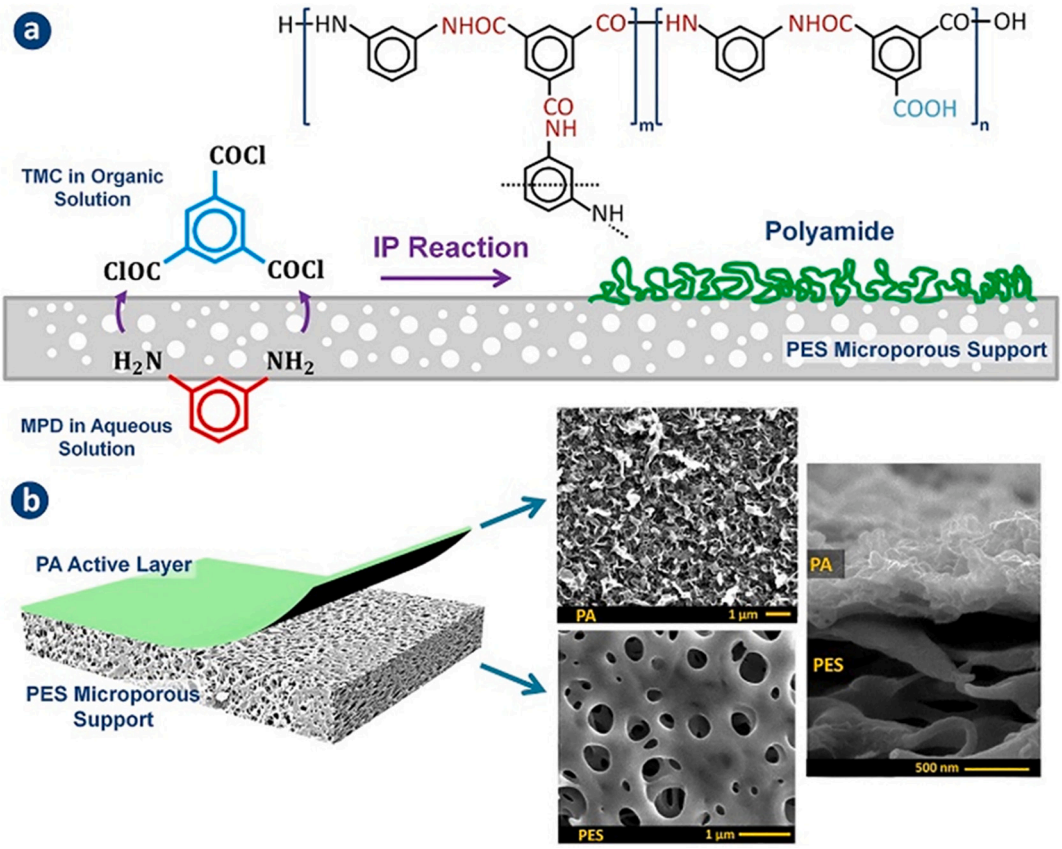

Fig. 1. (a) Illustration of the IP reaction between MPD and TMC at the surface of a polyethersulfone (PES) microporous support and the chemical structure of the polyamide layer [177]. The m and n in polyamide structure represent the crosslinked and the linear sections, respectively (m + *n* = 1). (b) Structure of the synthesized polyamide RO membrane with the top and cross-sectional morphologies [177]. Reproduced with permission from Springer Nature under the Creative Commons Attribution 4.0 International License. Color version of figure can be found online.

1. Introduction

Potable and clean water is becoming scarcer worldwide [1–3]. In order to meet the demand of potable and reusable water, numerous techniques are currently being employed, including filtration, sedimentation, distillation, and membrane-based separations such as reverse osmosis (RO), nanofiltration (NF), ultrafiltration (UF), and microfiltration (MF) [4–6]. Among these techniques, RO has gained significant attention due to its excellent desalination performance and simple operation [7]. In RO membranes, the solutes, which are generally monovalent salt ions, are separated by a non-porous layer via size exclusion and charge repulsion between the ionized solutes and membrane surfaces [8]. In order to have an efficient treatment of saline water, the ideal RO membranes should have high water permeance and be impermeable to solutes [8].

The first case of the fabrication of RO membranes was reported in 1959 by Reid and coworkers [9]. They were able to successfully synthesize a cellulose acetate membrane to remove salts from water. The fabricated membrane showed very good NaCl rejection (98%) [9]. However, the water permeance of the membranes was low (< 0.03 L/m^2/h/bar (LMH/bar)) [9]. Later, with an aim to improve the water permeance, Loeb and Sourirajan were able to fabricate a cellulose acetate membrane which exhibited improved water permeance (0.14 LMH/bar) along with good NaCl rejection (99%) [10]. Although some of the fabricated cellulose acetate membranes showed acceptable performance, the application of this membrane was limited due to its low thermal stability and chemical resistance [11,12], which influenced researchers to conduct more studies to synthesize membranes with better thermal and chemical properties. Then in 1971, Richter et al. suggested the application of aromatic polyamide membranes as an alternative, which had a better chemical and biological stability [13,14]. Although the water permeance from this membrane was found to be lesser (0.01 LMH/bar) than the cellulose acetate membranes, it exhibited a comparable NaCl rejection (99%) [14]. Later in 1979, a major milestone was achieved when Cadotte introduced polyamide thin film composite (TFC) membranes [15]. The polyamide membrane was produced from the interfacial polymerization of m-phenylenediamine (MPD) and trimesoyl chloride (TMC) on a microporous polysulfone (Psf) support, which was supported by a non-woven polyester fabric [15]. Compared to the cellulose acetate membranes, the fabricated polyamide membrane showed a higher water permeance (0.73 LMH/bar) and a similar NaCl rejection (99%). This membrane also had better stability in acidic and alkaline environments [15].

After achieving the groundbreaking success of the TFC membrane via the introduction of the interfacial polymerization (IP) reaction between the aromatic amine and aromatic acyl chloride, the research and investigation on new chemistries for polymeric RO membranes have been significantly reduced [16]. Current RO membranes in the market are still mostly based on the polyamide chemistry that has been developed several decades ago, i.e., the interfacial polymerization of MPD and TMC [16].

Although no new polymeric materials for RO membranes have been introduced, the performance of the RO-TFC membrane, specifically water permeance and salt rejection, has been dramatically improved [16]. The alteration of monomers [16–18], synthesis parameters [16,18], module structure [19], supporting layers [20–26], and the introduction of different nanomaterials [16,18,19,27–29] has resulted in the improvement of RO membrane performance [30–32]. The goal of

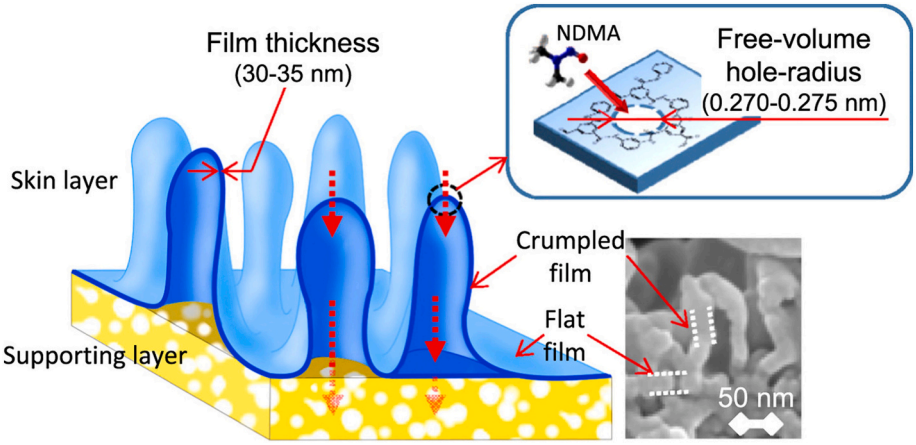

Fig. 2. Illustration of a RO membrane with a field emission-scanning electron microscopy cross-sectional image of an ESPA2 RO membrane [171]. Reproduced with permission from Elsevier. Color version of figure can be found online.

any modification is to push the boundaries of permeability/selectivity trade-off [33], although selectivity is the more critical factor to improve [34]. In addition, a better understanding of the RO membrane porous structure and surface, characterized by different techniques, has played a significant role in improving the RO membrane performance [19,29,35]. For instance, the application of atomic force microscopy (AFM) revealed that the roughness of the RO membrane could affect the water permeance and salt rejection of the membranes [36].

Even though the fabrication of RO TFC membranes in industrial settings is well established, there are numerous published variations to the protocol to synthesize fully aromatic polyamide RO membranes at the laboratory scale. When searching the literature, there appears to be no standardized protocol for RO membrane fabrication. The goal of this review is to help guide researchers wanting to synthesize fully aromatic polyamide separation layers on a laboratory scale. We reviewed over 130 papers from 2016 to 2020 and have compiled the various ways fully aromatic polyamide RO membranes have been synthesized [22,23,37–165]. This review is broken down into each step of the IP process with a summary of the techniques and conditions used for each step.

2. Synthesis of fully aromatic polyamide membranes

2.1. Mechanism of the interfacial polymerization reaction

There are several proposed mechanisms for the IP reaction to form polyamide RO membranes [164,166–172]. Several researchers have suggested that the IP reaction takes place in the organic phase by the diffusion of the amine monomers from the aqueous phase, as the acid chloride monomers have a highly unfavorable partition coefficient in the aqueous phase [166,167]. As a result, the mixing rate of the reactants, specifically the mass transfer rate of amine molecules towards the organic phase, governs the reaction rate of IP and affects the morphology and microstructure of the polyamide separation layer and the resultant membrane performance [166,167,173,174]. By nature, the IP reaction is very fast due to the high reactivity of the acid chloride monomers. However, the reaction rapidly begins to slow down significantly as the diffusion of the MPD monomers towards the organic phase is slowed due to the formation of the polyamide layer (i.e., a semi self-limiting reaction) [168]. The polyamide layer is considered to contain two layers: a dense and highly crosslinked base polyamide layer, which

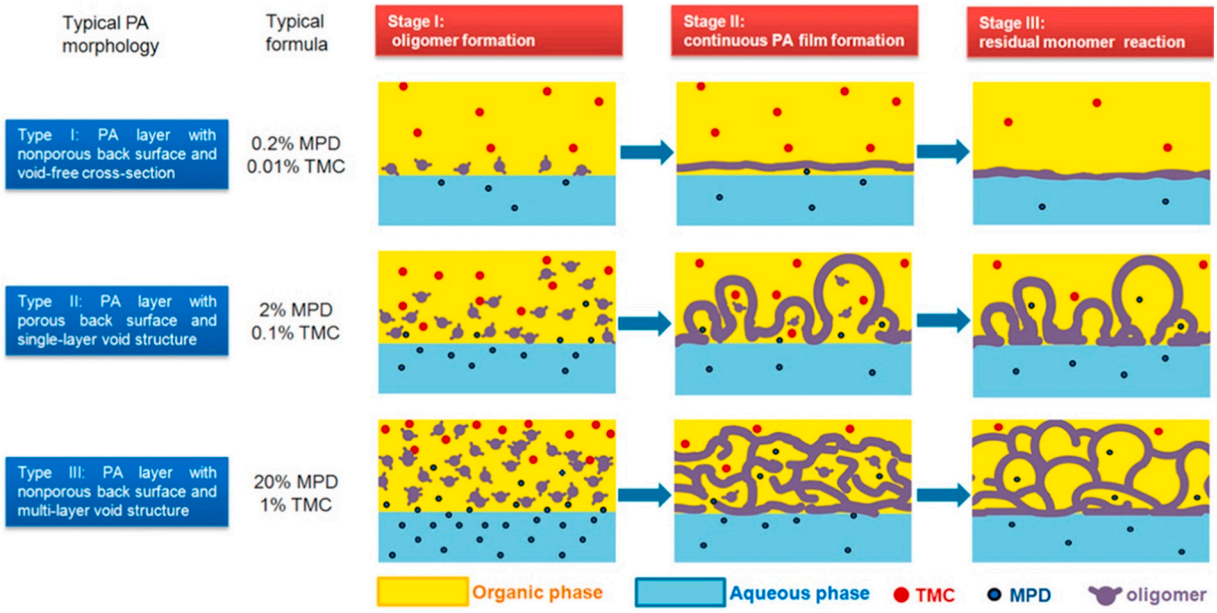

Fig. 3. Illustration of the formation mechanism of the polyamide layer using varying monomer concentrations [172]. Reproduced with permission from Elsevier. Color version of figure can be found online.

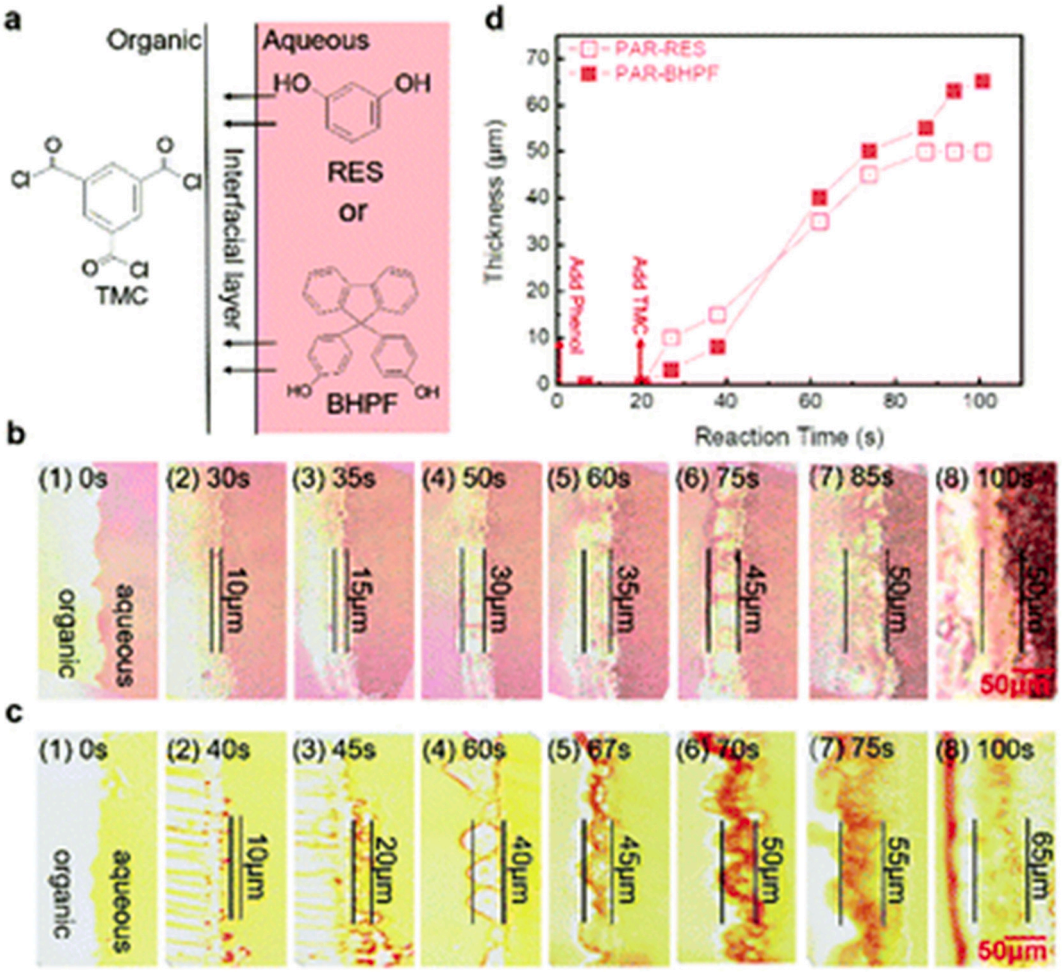

Fig. 4. (a) Schematic of the interfacial polymerization between resorcinol (RES) and 9,9-bis(4-hydroxyphenyl) fluorene (BHPF) with TMC, (b) polyarylate film formation between RES and TMC over time, (c) polyarylate film formation between BHPF and TMC over time, and (d) plot of polyarylate film thickness versus time. Reproduced from [183] with permission from The Royal Society of Chemistry. Color version of the figure can be found online.

is formed at the very beginning of the reaction (incipient layer), and a looser polyamide structure on top having the "ridge and valley" morphology [169]. Fig. 1 shows a general formation mechanism of the polyamide layer. It has been found that the polyamide layer has a surface roughness on the order of 100 nm due to the presence of "ridge-and-valley" structures, which increases the water permeance of the membranes due to the enhanced surface area [175,176].

Careful characterization of the "ridge-and-valley" structures revealed the presence of nanovoids in the polyamide layer [178]. Recently, Fujioka et al. performed the characterization of the polyamide layer using positron annihilation lifetime spectroscopy (PALS) and observed the free-volume hole-radius was 0.270–0.275 nm [170]. Fig. 2 shows the structure of the polyamide layer on top of the support membrane. The thickness of the polyamide layer and the free-volume holes of the polyamide layer play a crucial role in transporting water and solute (s) through the RO membrane [170]. Ma and coworkers suggested that the release of nanosized gas bubbles during the IP process, which they termed as nano-foaming, are responsible for those nanovoids [164,179]. The nanobubbles occur due to the heat generated by the IP reaction and are facilitated by the production of HCl, which reduces the solubility of dissolved gases such as CO_2, N_2, and O_2 [164,179]. In their study, Shen et al. found that using ultrasound during fabrication can produce a series of compression and rarefaction waves, and when the ultrasound becomes high, the rarefaction forces surpass the intermolecular interactions of the medium and produce cavitation bubbles on the medium [167,180]. However, these cavitation bubbles are unstable and can collapse suddenly, which produces a large amount of heat and high pressure. The generation of energy improves the mass transport of amine monomers, enlarges the mixing area, and accelerates the IP reaction [167,180]. The RO membrane fabricated using ultrasound showed better performance (water permeance was 3.44 LMH/bar and NaCl rejection was 95.9%) than the control RO membrane (water permeance was 1.99 LMH/bar and NaCl rejection was 94.7%) [167,180].

From previous studies, it has been found that the concentration of MPD and TMC can greatly affect the morphology of polyamide membranes. For example, An et al. observed that changing the MPD and TMC monomer concentrations affect the morphological parameters (such as surface curvature, Feret distance, thickness, perimeter, and area) of the crumple features of the RO membranes [171]. However, they did not investigate the effect of MPD and TMC concentration on the membrane performance [171]. In another study, Xu et al. tuned the MPD and TMC concentrations and found that the application of different concentrations of monomers results in membranes with three types of polyamide morphology [172]. Depending on the MPD and TMC concentration, the surface morphology showed different structures, including smooth, nodular, and leaf-like structures [172]. They used a MPD concentration ranging from 0.2 wt% to 20 wt% and found that a smooth, void-free structure formed at lower concentrations, a leaf-like, single-layer structure formed at moderate concentrations, and a nodular, multi-layer structure formed at higher concentrations [172]. Fig. 3 shows the formation mechanism of these three types of polyamide layers. They also found that the polyamide thickness depends on the morphology of the

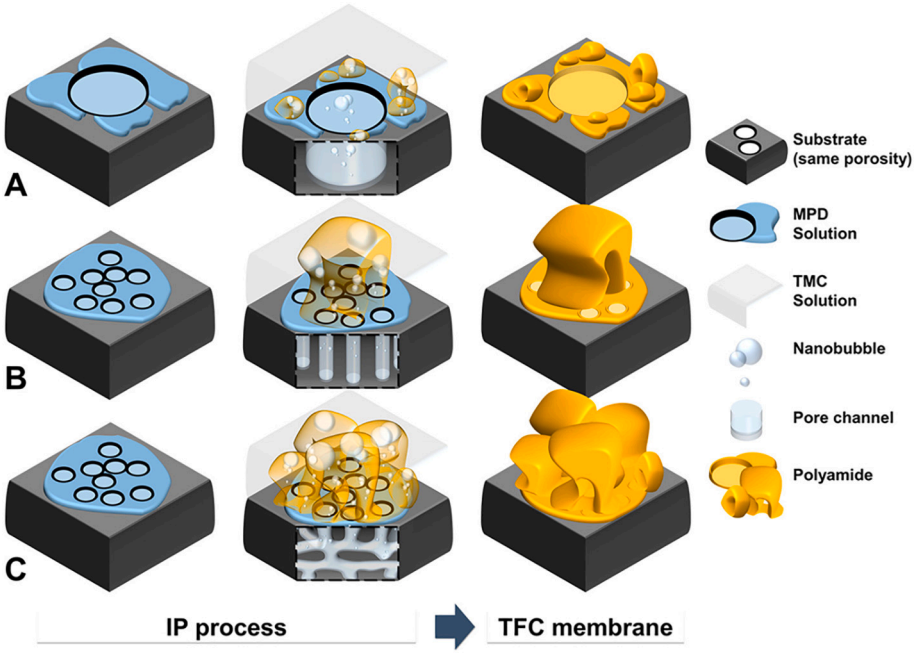

Fig. 5. Illustration of the role of the support membrane on the interfacial polymerization between MPD and TMC.

polyamide layers [172]. For example, in the case of the polyamide layers with a multi-layer void structure, the thickness of the polyamide layer was 361 ± 23 nm, which was almost 7-fold higher than the polyamide layer with a void-free cross-section (52 ± 6 nm) [172]. Among the above mentioned morphological features, the morphology with leaf-like structures (using moderate concentrations of MPD and TMC) showed the best membrane performance with a water permeance > 2.5 LMH/bar and a NaCl rejection > 95% [172].

Chowdhury et al. used electrospraying to synthesize polyamide layers [181]. The small droplet size and the low monomer concentrations used result in smoother and thinner polyamide layers than conventional polyamide layers. Fully aromatic polyamide layers of 15 nm thickness had a roughness of ~8 nm, a water permeance of 2 LMH/bar, and a NaCl rejection of 95.5% [181].

2.2. *Interfacial polymerization kinetics*

The kinetics of the interfacial polymerization reaction are challenging to study due to the very fast reaction (on the order of seconds) between MPD and TMC to form a thin film [182]. Nevertheless, there have been a few recent studies attempting to measure and model the kinetics of the interfacial polymerization reaction. Nawbahar et al. used microfluidic interferometry to measure the interfacial polymerization kinetics at a water droplet-oil phase interface [182]. By measuring the refractive index of the water droplet over time (i.e., as the reaction consumes MPD), the authors were able to track the spatial and temporal evolution of MPD concentration near the interface and determine its flux from the aqueous phase. The flux was related to the reaction to measure the reaction kinetics. They determined that the flux at the start of the reaction scales linearly with $[MPD]_0$ and $\sqrt{[TMC]_0}$ and the reaction has a rate constant of k = 110 L/(mol * s) [182]. However, as the polyamide

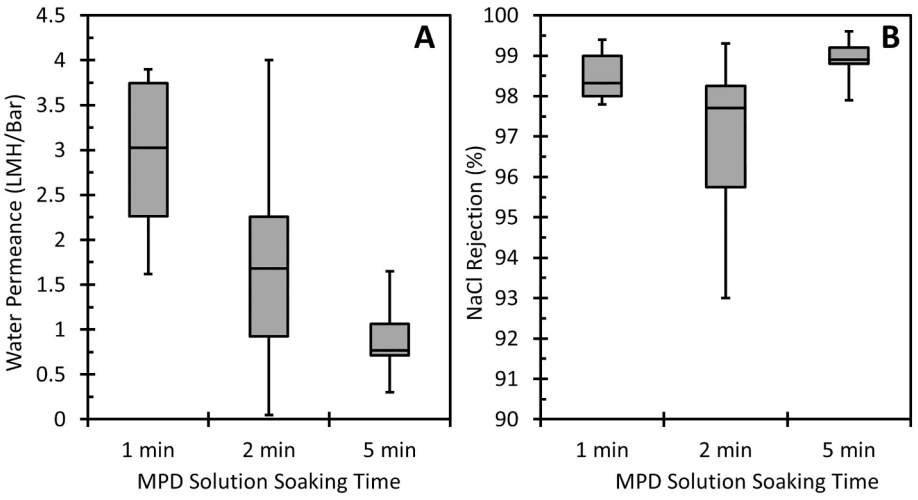

Fig. 6. Box-and-whisker plots of (A) water permeance (LMH/Bar) and (B) NaCl rejection for fully aromatic polyamide membranes synthesized with varying aqueous MPD solution soaking times. Specific synthesis conditions include an aqueous MPD concentration of 2 wt%, an organic TMC concentration of 0.1 wt%, and an organic TMC reaction time of 1 min.

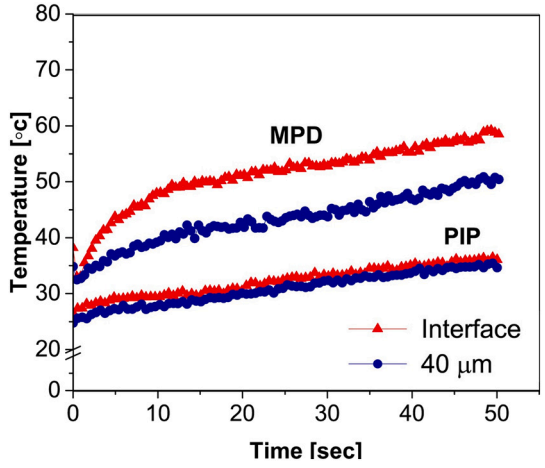

Fig. 7. Time evolution of the temperature close to the interface and 40 μm into the aqueous phase using MPD and piperazine (PIP) as the aqueous amine monomers. Reproduced with permission from Elsevier [198]. Color version of figure can be found online.

network beings to form, the amine fluxes decay more rapidly than predicted with their model, thus providing evidence for the "self-limiting" behavior of the MPD-TMC reaction.

Ren et al. used time-dependent FTIR microscopy to investigate the mechanism and kinetics of the interfacial polymerization reaction resorcinol (RES) and 9,9-bis(4-hydroxyphenyl) fluorene (BHPF) with TMC [183]. They chose this polyarylate system instead of the MPD polyamide one because the alcohol-TMC reaction is much slower than the amine-TMC reaction and the length of one FTIR measurement was ~6.7 s. Fig. 4 shows that with the microscopy, they were able to see the evolution of a film, including the reaction between BHPF and TMC forming bubbles. Using FTIR, they were able to see a clear depleting of the monomer peaks and a clear increase in the polyarylate peaks. They determined that the reaction kinetics scales linearly with $[RES]_0$ and $\sqrt{[TMC]_0}$ and the reaction has a rate constant of k = 119 L/(mol * s) [183], similar to that found by Nawbahar et al.

Li et al. used low coherence interferometry (LCI) to study the film-formation kinetics of the interfacial polymerization between MPD and TMC on a polysulfone support membrane [184]. They soaked the support membrane in a MPD solution and flowed the TMC over top of the membrane where it was subject to LCI. The used the surface-averaged intensity (SAI) profiles from the LCI to interpret the film-formation kinetics [184]. The initial SAI profiles provided evidence for incipient film formation, in which the polyamide is rapidly generated. This is followed by a slowdown of the growth of the polyamide network, which is seen by the abrupt change in the SAI increase rate. Then, the long period of nearly constant increase in the SAI is indicative of a diffusion-controlled, self-limiting growth [184]. However, they did not provide any data for a suggested rate constant of reaction.

Behera and Akkihebbal pH-metry to study the interfacial polymerization of MPD and TMC in an emulsion [185]. The basic principle of pH-metry is to measure the pH changes in the aqueous phase caused by the reaction (HCl formation) to monitor the progress of reaction. This is an extension of their previous studies using this technique [186–188], where in this study, they combine their previous methods to account for HCl generation from both the MPD-TMC reaction and from TMC hydrolysis. They found the kinetics fit a power law type, and they show that the reaction is approximately first order in the acid chloride group concentration and order 1.6 in the amine group concentration [185]. The authors found that when a surfactant is present, the rate of the reaction approximately doubles [185]. They noted that the reaction usually stops well short of 100% conversion of the stoichiometrically limiting monomer, and they attributed this to the lowering of pH which restricts the availability of the aqueous phase monomer at the reaction interface. Because the reaction takes place in the organic phase, only unprotonated amines can partition into the organic phase and react. As the pH is lowered, the amines begin to protonate and cannot partition into the organic phase and react. The authors do mention this pH-metry technique is not sensitive enough for high conversions.

2.3. Support effects

The membrane support used to synthesize the polyamide layer on top of plays a critical role in how the resultant polyamide membrane performs. The support effects have been the focus of a recent 2017 review [20], thus the discussion below will center on a few studies since then. A recent study by Elfa Peng et al. investigated the effect of support membrane pore size on polyamide layer structure and performance [189]. They used polycarbonate (PC) track-etched membranes with a pore size ranging from 10 to 900 nm as the membrane support. The top surfaces of polyamide films showed significant leaf-like roughness features for TFC membranes synthesized on 80 and 100 nm PC supports. Increasing the PC pore size resulted in less of these features forming. Decreasing the PC pore size resulted in a smoother polyamide layer. Not surprising, as the pore size of the PC increased, the water permeance increased [189]. The NaCl rejection of the membranes was compromised at PC pore sizes above 100 nm, likely due to defects forming in the polyamide layer over the pores and the polyamide layer over the rupturing when pressure is applied [189]. When the authors synthesized fully aromatic polyamide membranes on top of polysulfone (Psf) or PES support membranes both the water permeance and salt rejection were greatly improved, and as Fig. 5 shows, they suggested the interfacial polymerization processes is more effective on sponge-like support membranes [189]. The authors connect the PC pore size to the confinement effects from their previous studies referenced above ([164,179]) for the nanobubbles to escape during polyamide formation. Sharabati et al. found similar results when synthesizing polyamide layers on Psf supports with pore sizes ranging from 18 to 120 nm [24]. As the pore size decreased, the salt rejection increased, with Psf pore sizes below 40 nm producing polyamide layers with salt rejections above 95% [24].

Zhang et al. investigated the effect of Psf support porosity on the fully aromatic polyamide membrane thickness and performance [25]. The authors synthesized their own Psf membranes with varying porosity from 63 to 80%. They found that as the support porosity increased, the resultant polyamide layer water permeance decreased and the salt rejection increased [25]. The authors suggested that the polyamide layers synthesized on the lower porosity supports could delaminate easily, resulting in lower salt rejection. Additionally, as the support porosity increased, the polyamide layer roughness and thickness also increased [25], which is similar to what was found by Wang et al. [23]. These studies indicate that there is an optimum support porosity (70–80%) and pore size range (~20–80 nm) for fabricating high salt rejecting polyamide membranes.

Finally, Aghajani et al. investigated the effects of porous support resistance of commercial fully aromatic polyamide membranes [21]. Unsurprisingly, at low transmembrane pressures, they found that the support membrane resistance is negligible compared to the polyamide membrane. However, at higher transmembrane pressures (up to 8.3 MPa), the support increased the overall membrane resistance by ~30% [21]. It would be worthwhile to further investigate this issue for applications where even higher transmembrane pressures are needed.

For the purposes of this study, the results discussed below will pertain only to membranes synthesized on Psf or PES supports. Psf supports with a molecular weight cut-off of ~20–30 kDa dominate the MPD-TMC based membrane literature and the commercial membrane products and provide the platform for our investigation of the polyamide layer synthesis parameters.

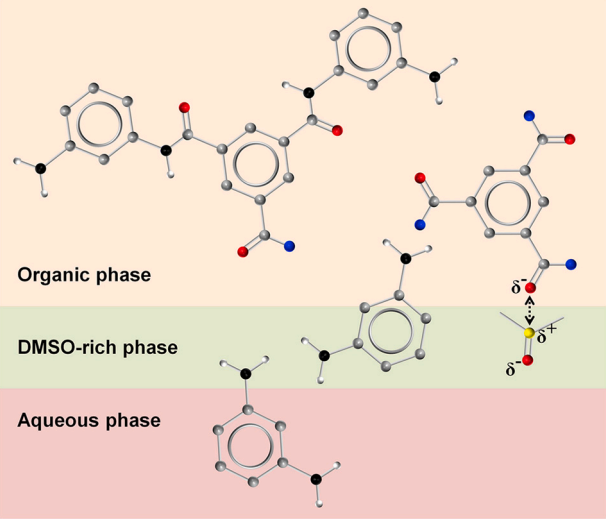

Fig. 8. The effect of using a DMSO co-solvent in the aqueous phase on the interfacial polymerization reaction. Reproduced with permissions from Elsevier [162]. Color version of figure can be found online.

2.4. Reaction conditions

The synthesis parameters which are considered vital for fabricating the TFC membranes are the MPD and TMC monomer concentrations, MPD soaking time, and MPD-TMC reaction time. In this section, we discuss the effect of each synthesis parameter on the membrane performance. Additionally, we discuss the correlation between MPD and TMC concentration (i.e., MPD/TMC ratio), MPD concentration and MPD soaking time, and MPD soaking time and MPD-TMC reaction time in Sections 2.4.1, 2.4.3, and 2.4.4, respectively.

2.4.1. MPD and TMC concentration

Several studies have suggested that the surface properties and membrane performance of TFC polyamide membranes can be altered by the MPD and TMC monomer concentrations used in the IP reaction [54,171,172,190–193]. In the reviewed papers, the concentration of MPD in the aqueous solution ranged from 0.01 to 4.6 wt% and, the concentration of TMC in the organic solution ranged from 0.001 to 10 wt %. The most common MPD and TMC concentrations were 2.0 wt% and 0.1 wt%, respectively. Unfortunately, there is not enough data from membranes synthesized with common conditions to adequately analyze the effects of MPD and TMC concentrations across numerous papers. Therefore, our discussion below will center around individual lab studies. Xu et al. found that the concentration of MPD and TMC and MPD/TMC ratio greatly impacted the membrane performance [172]. By changing the MPD concentration from 0.1 to 20.0 wt% while keeping the TMC concentration constant at 0.1 wt%, the membrane fabricated using 2.0 wt% MPD had the highest water permeance of 4.0 LMH/bar and NaCl rejection of 99.5% [172]. When the authors used low MPD (0.2 wt%) and TMC (0.1 wt%) concentrations, they noticed semi-smooth and continuous surface morphology [172]. The membranes made with a MPD concentration between 1 and 4 wt% (using 0.1 wt% TMC) exhibited a leaf-like structure [172]. Increasing the MPD concentration to 20 wt% (using 0.1 wt% TMC) showed a continuous polyamide layer with a stick-like structure [172]. By changing the TMC concentration from 0.01 to 1.0 wt% while keeping the MPD concentration constant at 2.0 wt%, the membrane fabricated using 0.1 wt% TMC had the highest water permeance of 4.0 LMH/bar and NaCl rejection of 99.5% [172]. In order to understand the effect of monomer concentration and other synthesis parameters, most experimental trials were performed using the one-factor-at-a-time method, where only a single factor was modified in each trial [190]. Chai et al. found that the thickness of the polyamide layer increases with the TMC concentration [191]. The authors found the membrane surface to be smooth and featureless when they used a lower TMC concentration [191]. When the TMC concentration was increased, the polyamide layers were more cross-linked and had a higher surface roughness [191]. Increasing the TMC concentration shifted the rate-controlling step from being diffusion-controlled in the organic phase to being diffusion-controlled in the polyamide film [191]. This shift led the IP process towards being self-limiting, where the formation of a dense cross-linked barrier prevented the MPD molecules from reacting with TMC molecules [191]. Though there was a significant change in polyamide layer thickness when the TMC concentration was changed, the investigators did not see any apparent change in thickness when the MPD concentration was increased [191]. In contrast, Roh et al. found that the polyamide film thickness increased when both the MPD and TMC concentrations increased [192]. The MPD concentration was found to impact the polyamide layer thickness more than the TMC concentration [192]. When the TMC concentration was increased from 0.01 to 0.1 wt/v%, the NaCl rejection of the membrane was increased by 6% from 90%, whereas the water permeance was decreased by 3% from 8.20 LMH/bar. Increasing the TMC concentration from 0.01 to 1 wt/v% resulted in an increase of the polyamide layer thickness by 360% [192]. When the MPD concentration was increased from 0.01 to 1 wt/v%, the thickness of the active layer increased [192]. Increasing the MPD concentration from 0.01 to 0.1 wt/v% dramatically decreased the water permeance by 24% from 11.41 LMH/bar and the NaCl rejection increased by almost 20% from 78% [192]. Increasing the MPD concentration than 0.1 to 1 wt/v% decreased the water permeance by 38%, and the NaCl rejection was consistent at 95% [192]. In addition to the changes in the thickness of the polyamide layer, the authors observed that the MPD and TMC concentrations played a role in polyamide layer hydrophilicity [192]. Increasing the TMC concentration increased the hydrophilicity, whereas increasing the MPD concentration decreased the hydrophilicity [192]. Xie et al. found there is an optimum MPD concentration of approximately 1.5 wt% to obtain a high water permeance (> 2 LMH/bar) [193]. Increasing the MPD concentration from 1.5 wt% to 3 wt% at constant TMC concentration enhanced the driving force of the diffusion of MPD molecules and reduced the water permeance by 24.6% [193]. Changing the MPD concentration did not affect the salt rejection significantly in their study [193].

In another study, Khorshidi et al. found that at higher MPD concentrations and constant TMC concentration, the water permeance decreased from 5.21 to 2.79 LMH/bar [190]. The higher MPD concentrations enhanced the driving force for the diffusion of the MPD molecules, increased the polyamide layer thickness with bigger ridge-and-valley structures, and reduced the water permeance [190]. When the TMC concentration was increased from 0.15 to 0.35 wt% at constant MPD concentration, the water permeance was increased from 1.38 LMH/bar to 5.21 LMH/bar, and the NaCl rejection decreased from 96.9% to 91.4% [190]. The authors assumed that the membrane performance of their synthesized RO membranes not only depends on the cross-linking density but also depends on the thickness of the loose polyamide structure [190]. Reducing the MPD/TMC concentration ratio by increasing the TMC concentration made the polyamide layer denser, increased the cross-linking density, and reduced the driving force for the diffusion of the MPD molecules [190]. At higher TMC concentrations, a thin polyamide layer with nodular structures was formed instead of a looser polyamide layer with a ridge-and-valley structure [190]. Thus, even though the membrane with a lower MPD/TMC concentration ratio had higher cross-linking density, the water permeance was higher due to the formation of a thinner polyamide layer [190]. When Song et al. increased the MPD and TMC concentrations and kept the MPD/TMC concentration ratio constant at 10, the water permeance decreased and the NaCl rejection increased [54]. Xu et al. made fully aromatic RO membranes with different MPD and TMC concentrations, and they found that when the membranes were fabricated with a 1–4 wt% MPD concentration, a 0.05–0.2 wt% TMC concentration, and a MPD/TMC

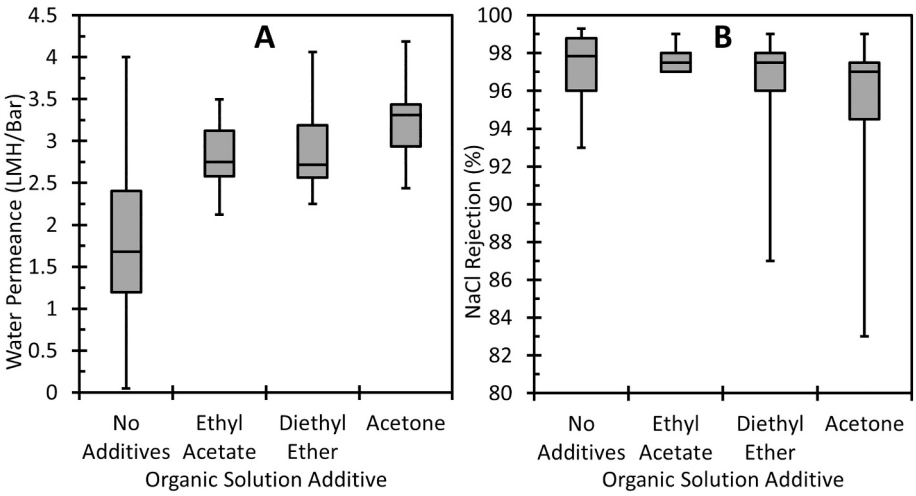

Fig. 9. Box-and-whisker plots of (A) water permeance (LMH/Bar) and (B) NaCl rejection for fully aromatic polyamide membranes synthesized without additives and with co-solvents (additives) in the organic solution. Specific synthesis conditions include an aqueous MPD concentration of 2 wt%, an aqueous MPD solution soaking time of 2 min, an organic TMC concentration of 0.1 wt%, and an organic TMC reaction time of 1 min.

concentration ratio in the range of 10–40, the produced membranes showed a good water permeance > 2.5 LMH/bar and NaCl rejection > 98% [172]. They observed the effect of MPD and TMC concentration on the formation of the polyamide layer and porosity of the back surface of the polyamide layer, which results in changes in membrane performance. When the MPD concentration was lower than 1 wt%, the RO membranes had a lower water permeance of 1.39 LMH/bar due to the formation of a non-porous back surface with a void-free cross-section [172]. When the MPD concentration was in the range of 1–4 wt%, the resultant membranes had higher water permeance values due to the formation of single-layer void structures with porous back layers [172]. When they used a MPD concentration of 20 wt%, the water permeance was zero due to the formation of a non-porous back layer with a multi-layer void structure [172].

2.4.2. Aqueous and organic phase solution volumes

Most articles do not report the solution volumes used in either the aqueous or organic phase for the interfacial polymerization process. Additionally, the membrane area is not always reported with the solution volume(s) either [23,55,58,63,72,74,77,86,106,110]. Some articles only report the aqueous MPD solution volume but not the organic TMC solution volume [55,139]. Some articles are the opposite, where they only report the organic TMC solution volume but not the aqueous MPD solution volume [45,110,135,155]. Reported aqueous MPD solution volumes can range from 10 mL to 100 mL [23,40,44,55,58,63,72,74,77,83,86,89,92,97,104,106,111,117,118,139]. The average aqueous MPD solution volume per membrane area is 0.20 mL/cm^2 [40,44,83,89,92,97,104,111,117,118]. Reported organic TMC solution volumes can range from 10 mL to 100 mL [23,40,44,45,58,63,72,74,77,83,86,89,92,97,104,106,110,111,117,118,135,155]. The average organic TMC solution volume per membrane area is 0.24 mL/cm^2 [40,44,83,89,92,97,104,111,117,118,135,155]. Even though the applied volume of the aqueous solution is not the volume that participates in the interfacial polymerization reaction due to the removal of the excess aqueous MPD solution (see Section 2.5.1), the aqueous and organic solution volumes and the membrane area the solutions are contacting needs to be reported to adequately reproduce the synthesis protocol. Additionally, the precise method for using each solution needs to be described. In almost all cases, some sort of seal, whether a gasket, ring, or tape, is used so that the organic TMC solution only contacts the top surface of the membrane. However, there are two approaches used with the aqueous MPD solution. In some cases, the same sealing approach as the organic TMC solution is used, but other times the support membrane is completely immersed in aqueous MPD solution. Xie et al. did an excellent job of reporting the solution volumes and membrane area used, and they provided pictures to show their exact process used [193].

2.4.3. MPD soaking time

MPD soaking time is a very important part of the RO membrane synthesis process. The soaking of amine monomers affects the morphology of the polyamide separation layers. Inefficient soaking can lead to the formation of pinholes on the separation layer, which results in substandard RO membrane performance [193]. The most common MPD soaking time is 2 min [22,37–39,41,44,49,52,55,57–59,67,71,73,77,79,83,86,87,90–92,95,97,111,115,116,119,125,126,134,137–141,146–148,150,151,158,164]. Fig. 6 shows the effect of MPD soaking time on the resultant membrane performance while keeping the MPD concentration, TMC concentration, and TMC reaction time constant with outliers removed (see Supporting Information for details). Statistical analyses (see Supporting Information for details) show that the polyamide membranes made using a 5 min MPD solution soaking time had a lower water permeance than the membranes made using a 1 min MPD solution soaking time, and the polyamide membrane made using a 2 min MPD solution soaking time had a lower NaCl rejection than the membranes made using 1 and 5 min MPD solution soaking times. It has been shown that by increasing the soaking time of the aqueous amine solution, the NaCl rejection increases and the water permeance decreases [194,195]. Zargar et al. found that when the amine soaking time increased from 2 to 10 min, the NaCl rejection increased from 84.3% to 91.9%, and the water permeance decreased slightly from 2.02 LMH/bar to 1.86 LMH/bar [194]. When a longer soaking time is used, the support membrane absorbs more MPD monomers and the monomers have a chance to penetrate deeper into its porous structure [193,194]. The impregnation of MPD monomers in the support membrane pores increases the availability of MPD molecules, which enhances the driving force for MPD diffusion towards the organic phase and results in the formation of a thick polyamide layer and the reduction of water permeance of the resultant RO membrane [193–195]. In another study, Vatanpour et al. immersed the supporting membrane in an aqueous MPD solution accompanied by additives, and they found that by increasing the MPD soaking time from 5 to 15 min, the NaCl rejection slightly increased, whereas the water permeance was significantly decreased [195]. The enhanced diffusion and absorption of the amine solution in the supporting membrane pores due to the increased MPD immersion time was responsible for the formation of a thick polyamide layer and

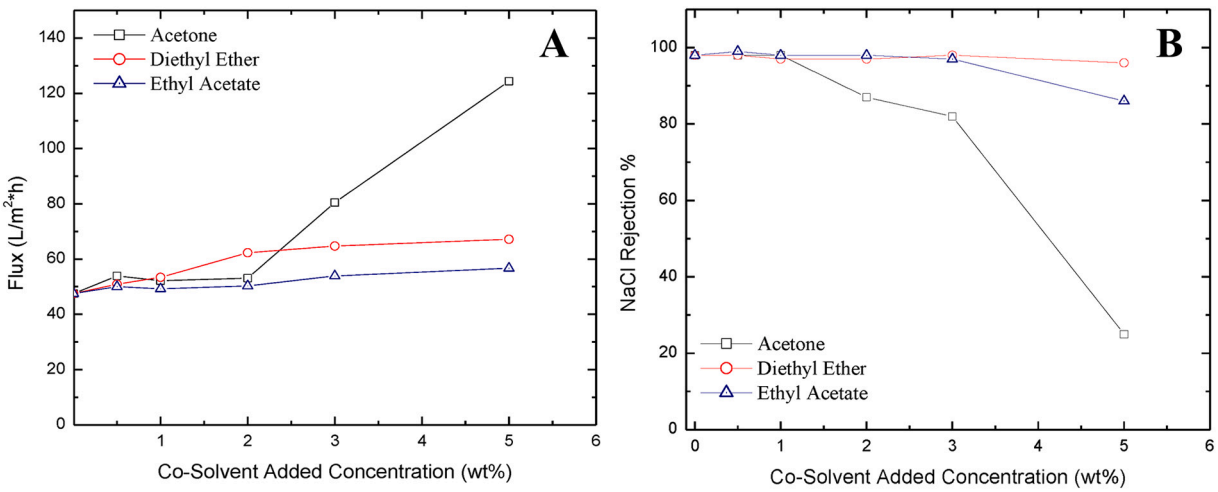

Fig. 10. Effect of using acetone, diethyl ether, and ethyl acetate in the organic phase on water flux (A) and NaCl rejection (B). Reproduced with permission from MDPI [148]. Color version of figure can be found online.

results in a decrease in water permeance [195]. The authors found that when the MPD soaking time is increased with increasing MPD concentration, the water permeance decreased [195]. The longer the MPD soaking time with a high MPD concentration leads to more MPD molecules available for absorption on the support membrane, which eventually leads to the formation of a thicker polyamide film, reduced availability of free –COOH groups, and thus, a reduction in the water permeance [195]. However, the authors did not observe much change in the salt rejection when they increased the MPD soaking time for different MPD concentrations [195]. In the study conducted by Zargar et al., it was observed that though longer MPD soaking times increases the penetration of amine monomers into the support layer porous network, the formed polyamide layer cannot highly diffuse inside the support membrane pores because of the restricted TMC supply to the supporting layer due to the limited solubility of TMC in water [193,194]. Thus, if the supply of TMC is limited, increasing the membrane soaking time does not significantly reduce the water permeance but greatly enhances the salt rejection [194].

2.4.4. *MPD-TMC reaction time*

In fully aromatic RO polyamide membrane synthesis, the MPD-TMC reaction time is a very important parameter that determines the extent of IP reaction. The most common reaction time found in the reviewed studies is 1 min. By tuning the reaction time, the RO membrane performance can be controlled. Unfortunately, there is not enough data from membranes synthesized with common conditions to adequately analyze the effects of MPD-TMC reaction time across papers. Therefore, our discussion below will center around individual studies investigating the effect of reaction time. For example, Vatanpour et al. studied the effect of the MPD-TMC reaction time on the membrane performance and found that by increasing the reaction time from 1 to 3 min, the water permeance and salt rejection are increased [195]. Increasing the reaction time led to an increase in the ratio of single bond -COOH to single bond -CONH. During the formation of the polyamide layer, the MPD

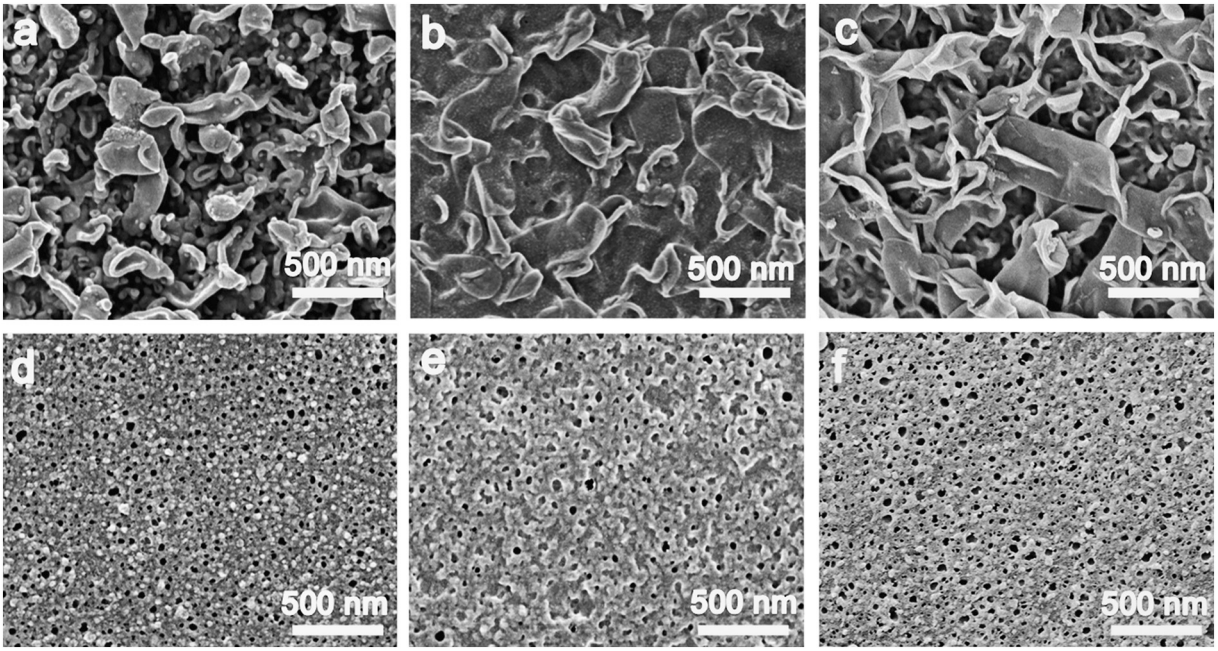

Fig. 11. SEM top surface and back surface of Hydranautics ESPA2 (a,d), Dow BW30 (b,e), and a homemade fully aromatic membrane (c,f). Reproduced with permission from Elsevier [40].

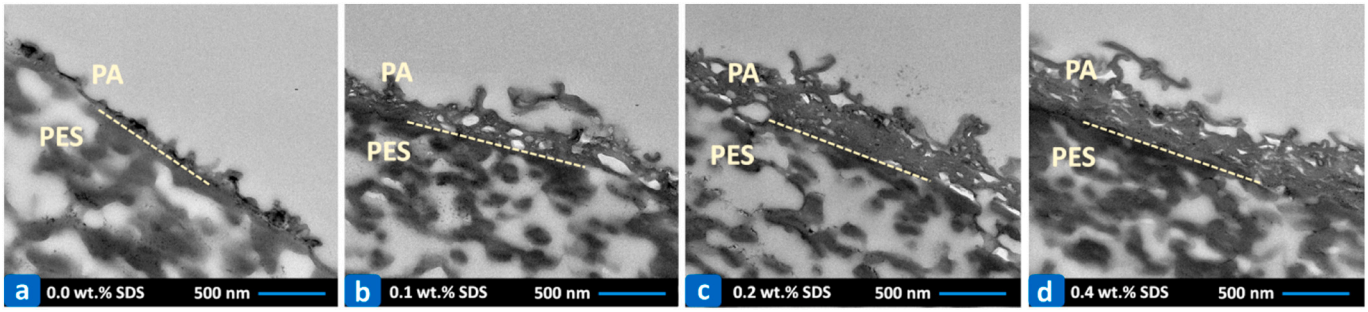

Fig. 12. Cross-sectional TEM images of fully aromatic polyamide membranes made with different concentrations of SDS. Reproduced with permission from Elsevier [161].

molecules initially diffuse to the organic layer, react with the -COCl group, and form the primary polyamide layer [195]. As time progresses, the remaining -COCl groups react with new entering MPD molecules and make the polyamide layer more cross-linked. After the formation of the primary layer and during the film growth, the diffusion rate of the MPD molecules becomes slower comparing to the diffusion rate of TMC [195]. Thus, the -COOH groups of unreacted TMC molecules becomes more available, which enhances the water permeance of the membrane [195]. When Kadhom et al. studied the effect of MPD-TMC reaction time (5, 10, 15, 20, and 25 s at room temperature) on the membrane performance, they observed that by increasing the reaction time, the water permeance decreased due to the increased thickness and cross-linking of the polyamide layer [196]. However, the NaCl rejection remained approximately the same for all reaction times, which was attributed to the fast nature of the IP reaction [196]. Due to rapid reaction, the polyamide layer reduced the MPD transfer towards the TMC organic solution [196]. As a result, no significant change was observed in salt rejection for different reaction times [196]. A reaction time of 5 s provided the best water permeance when it was compared with other reaction times [196]. At shorter reaction times, some of the TMC molecules might not react with MPD, and the unreacted -COCl groups of TMC was hydrolyzed to -COOH groups [196]. The formation of -COOH groups increased the hydrophilicity, and thus, improved the water permeance [196]. The authors also investigated the effect of increasing MPD soaking time from 10 to 30 s on the membrane performance for reaction times of 5 to 25 s [196]. They found that when the reaction time was 5 s, increasing the MPD soaking time did not change the water permeance or salt rejection significantly [196]. However, in the case of other reaction times (10 s, 15 s, 20 s and 25 s), when increasing the MPD soaking time, the salt rejection was increased [196]. When the reaction time was 10, 15, 20, and 25 s, with increasing MPD soaking time, the water permeance was increased [196]. According to the authors of the study, by increasing the MPD soaking time, the MPD molecules react more with the support, and one or both of the amine groups of MPD molecules may get oxidized, which eventually makes the surface more hydrophilic [196]. However, in the case of 15 s and 20 s reaction time, increasing the MPD soaking time above 25 s reduced the water permeance, which might happen due to the reduction in the availability of–COOH groups [196]. In another study, Dong et al. noticed a decrease in water permeance and an increase in NaCl rejection when they performed the reaction for a longer time [197]. For the reaction time below 12 s, the water permeance was 4.70 LMH/bar and the NaCl rejection was 98.5% [197]. Increasing the reaction time to 15 s resulted in a slightly lower permeance of 4.54 LMH/bar and a similar NaCl rejection of 98.7% [197]. When the reaction time was further increased, the permeance was reduced to 4.06 LMH/bar and the NaCl rejection was similar at 98.9% [197].

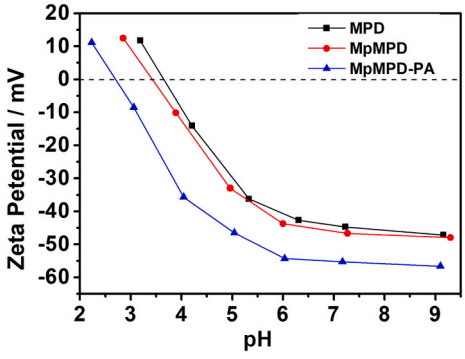

Fig. 13. Zeta potential of an MPD-TMC membrane (MPD) and two other modified chemistry membranes (MpMPD and MpMPD-PA). Reproduced with permission from Elsevier [59]. Color version of figure can be found online.

2.4.5. Reaction temperature

In almost all cases, the temperature of the aqueous and organic solutions is not reported. It is therefore assumed that the solutions are approximately at room or ambient temperature [37,38,87,91,97,98,149,150,160], likely 20 to 25 °C [75,146,154,163]. MPD solubility and diffusivity in the organic solution changes with temperature, and thus, impacts the properties of the resultant polyamide layer [169]. Ghosh et al. used four organic Isopar-G solution temperatures between 8 and 38 °C [169]. They found that as the temperature of the Isopar-G solution increases, the water permeance remains approximately the same from 0.02 LMH/bar at 8 °C to 0.03 LMH/bar at 38 °C, the salt rejection decreases from ~98% at 8 °C to ~93% at 38 °C, the surface hydrophobicity slightly increases, and the surface roughness increases [169]. Bera et al. used an aqueous MPD solution temperature of 60 °C and an organic TMC solution temperature of 30 °C for interfacial polymerization [157]. The produced membrane had a water permeance of 3.6 LMH/bar and a NaCl rejection of 96% [157]. Khorshidi et al. used eight organic hexane solution temperatures between −20 and 50 °C for interfacial polymerization [177]. They found that decreasing the organic solution temperature led to a decrease in polyamide layer thickness, an increase in cross-linking density, an increase in hydrophilicity, a decrease in surface roughness, a decrease in NaCl rejection from 99% at 50 °C to 94% at −20 °C and an increase in water permeance from 1.3 LMH at 50 °C to 5.6 LMH/bar at −20 °C [177]. Interestingly, the water permeance was lowest (0.7 LMH/bar) at 25 °C. Ali et al. synthesized polyamide membranes using organic Isopar-G solution temperatures of 20, 60, and 100 °C [163]. They found the surface roughness increased, the polyamide layer increased, the water permeance decreased slightly from 0.83 LMH/bar at 20 °C to 0.75 LMH/bar at 100 °C, and the NaCl rejection increased very slightly from 99.2% at 20 °C to 99.6% at 100 °C as temperature increased [163]. Zhao et al. soaked the support membrane in a room temperature MPD solution and then dipped the MPD-soaked membrane in a TMC solution in an ice bath of ~10 °C [38]. The resultant membrane had a water permeance of 1.76 LMH/bar and a NaCl rejection of 98.2% [38]. Ma et al. used a different

approach to change the temperature of the interfacial polymerization [164]. The authors soaked the porous substrate in MPD, stored it at −16 °C for 30 min, then poured the TMC solution on the frozen substrate [164]. This membrane was not tested for desalination performance but was characterized by scanning electron microscopy (SEM). The SEM image showed a relatively smooth surface almost free of leaf-like or nodular structures [164]. Recently, Ukrainsky and Ramon attempted to measure the temperature of the interfacial polymerization reaction zone by utilizing a temperature-sensitive fluorescent dye [198]. As shown in Fig. 7, the authors found that the temperature of the IP was at least 50 °C, with many configurations being above 70 °C and the maximum temperature reached of 86 °C [198].

2.4.6. Additives

Additives are commonly used in the aqueous or organic phase of the interfacial polymerization process for improving membrane performance by altering monomer solubility, diffusivity, and hydrolysis [169]. There has been a lot of work on using nanomaterials in the IP process to improve RO membranes that have been recently reviewed [16,18,19,27–29,199], however, the use of nanomaterials is out of the scope of this review. Additionally, the use of alternative monomers or other compounds that become part of the polyamide layer is also out of the scope of this review [16–18,29,199]. This section will review the most commonly used additives in the aqueous and organic phases.

2.4.6.1. Aqueous phase additives. Surfactants, co-solvents, and other additives have been used in the aqueous phase of the IP process to improve membrane performance [19,169]. Unfortunately, there is not enough data from membranes synthesized with common conditions to adequately analyze the effects of aqueous additives across papers. Therefore, our discussion below will center around general information from studies using aqueous additives with a few individual studies discussed in detail. The most common organic additives used in the aqueous phase are triethylamine (TEA) at a concentration of 0.3–4.2 wt % [37,40,44–48,53,56,61,63,65,66,68,69,76,81,82,84,85,92,93,95,96,101–105,116,119,121,122,126,129,130,132,133,135,136,139,145,147,154,156,161,165] and (±)-camphor-10-sulfonic acid (CSA) at a concentration of 1–4 wt% [37,45,46,48,53,56,61,63,66,68,69,76,82,84,85,92,95,102,104,105,116,119,121,126,129,130,132,133,136,139,144,147,153,154,156,161]. TEA is most commonly used at 2 wt% and CSA is most commonly used at 2 wt%. TEA is an acid-acceptor that is used to neutralize the HCl produced during the IP reaction which accelerates the MPD-TMC reaction [47,48,102,119,139,154,161,169,199,200]. NaOH at a concentration of 0.05–0.6 wt% is another commonly used HCl neutralizing agent [52,99,153]. It is suggested that TEA also can influence the polycondensation rate by controlling the state of diamine dissociation [48,199,200]. CSA is suggested to improve the absorption of the amine solution in the support membrane [102,119,139,154,161,169,200], and CSA is suggested to protect the microporous skin layer of the support ultrafiltration membrane from annealing during curing [48,169]. TEA and CSA are almost always used together [37,45,46,48,53,56,61,63,66,68,69,76,82,84,85,92,95,102,104,105,116,119,121,126,129,130,132,133,136,139,147,154,156,161], with TEA occasionally being used by itself as an additive or a pH adjuster [40,81,93,96,101,103,135,145]. CSA was used only once without TEA but in the presence of sodium lauryl sulfate (SLS) [144].

Surfactants, most commonly sodium dodecyl sulfate (SDS) at a concentration of 0.05–2.0 wt% [37–39,44–48,53,56,63,65,68,69,85,91,92,105,116,122,134,136,153,161,165], are used in the aqueous phase of the IP process to improve membrane performance by improving the wettability of the support membrane [19,38]. It is suggested that the surfactants form a self-assembled network at the aqueous/organic interface allowing for fast, more homogenous diffusion of amine monomers across the interface [47,201]. The use of surfactants may lead to a more uniform pore size distribution in the polyamide layer. SDS is most commonly used at a concentration of 0.1 wt%. Sodium dodecylbenzenesulfonate (SDBS) at a concentration of 0.2 wt% [150] and SLS at a concentration of 0.1–0.15 wt% [119,126,144] also have been used as a surfactant in the IP process.

Co-solvents have been used to promote polyamide formation [199]. Fig. 8 shows that it is suggested that the use of co-solvents, such as dimethyl sulfoxide (DMSO) at a concentration of 0.5–5 wt% [63,136,147,153,157,162], forms a transition layer between the aqueous and organic phases which facilitates the IP process by improving the amine monomer diffusion [16,162,169,199]. DMSO is most commonly used at a concentration of 1.0 wt%. Lee et al. used DMSO at concentrations of 1, 2, 3, and 5 wt% to synthesize fully aromatic polyamide membranes [162]. At DMSO concentrations of 1 and 2 wt%, the water permeance was 6.00 LMH/bar and the NaCl rejection was 96.5% [162]. At DMSO concentrations of 3 and 5 wt%, the water permeance was 7.80 LMH/bar and the NaCl rejection was 78.0% [162]. As DMSO concentration was increased, the polyamide layer thickness, roughness, and cross-linking density decreased. When DMSO and glycerol were used as additives, the water permeance was 2.20 LMH/bar and the NaCl rejection was 95.5% [157]. When DMSO, CSA, SDS, glycerol, and NaOH were used as additives, the water permeance was 5.80 LMH/bar and the NaCl rejection was 99.0% [153]. 2-ethyl-1,3-hexanediol (EHD) is suggested to facilitate MPD transport to the organic solution [147,202]. When EHD was used at a concentration 0.2 wt% in the presence of DMSO, TEA, and CSA, the optimal membrane possessed a water permeance of 5.18 LMH/bar and a NaCl rejection of 87.8% [147,202].

One study by Khorshidi et al. used a Taguchi method to investigate the simultaneous effects of SDS, TEA, CSA, and DMSO on fully aromatic polyamide membranes [161]. The use DMSO, CSA, and TEA from 0.5 to 2 wt% fabricated polyamide membranes with a higher water permeance, while the use of SDS from 0.1 to 0.4 wt% fabricated polyamide membranes with a lower water permeance. Conversely, increasing the amount of SDS increased the salt rejection, while increasing the DMSO and TEA concentration decreased the salt rejection. Polyamide membranes fabricated with 1 wt% CSA had the highest salt rejection. The use of additives produced thicker and rougher polyamide layers with larger surface features [161]. By increasing only the SDS concentration, the resultant polyamide layer was thicker, rougher, more hydrophilic, and had a higher degree of cross-linking. By increasing only the DMSO concentration, the resultant polyamide layer was thicker, smoother, more hydrophilic, and had a higher degree of cross-linking. By increasing CSA concentration, the resultant polyamide layer was smoother, of similar hydrophilicity, and had a slightly lower degree of cross-linking. By increasing TEA concentration, the resultant polyamide layer was thicker, slightly rougher, of similar hydrophilicity, and had a slightly higher degree of cross-linking [161].

Inorganic salts are another aqueous phase additive that have been used. $CaCl_2$ is suggested to improve membrane hydrophilicity, and when it was used at a concentration of 0.01 wt% in the presence of TEA and CSA, the optimal membrane possessed a water permeance of 2.21 LMH/bar and a NaCl rejection of 96.3% [61]. Ma et al. used 6.0 wt% $NaHCO_3$ as a proton scavenger to enhance nanobubble formation during the IP reaction [164]. The resultant polyamide membrane had a rougher polyamide layer, a higher water permeance of 2.69 LMH/bar, and a higher NaCl rejection of 98.6% compared to the membrane made without $NaHCO_3$ [164].

2.4.6.2. Organic phase additives. Of the papers reviewed, only 5 used additives in the organic phase [57,82,140,147,148]. Co-solvents are the most commonly used additives in the organic phase. Dichloromethane (DCM) [57], dimethyl carbonate (DMC) [82], ethyl acetate (EA) [140,148], diethyl ether (DEE) [140,148], and acetone [148] have been used as organic co-solvents. When DCM was used as the only additive at 4 wt% in n-hexane, the membrane water permeance was 2.30 LMH/bar

and the NaCl rejection was 95.5% [57], similar to membranes made with no additives. When DCM at 4 wt% was combined with trimellitic anhydride chloride (TAC), an acid anhydride with relatively low reactivity that can be used as an acylating agent for amide bond formation, at a concentration range of 0.02 to 0.08 wt%, the membrane water permeance was 5.50 LMH/bar and the NaCl rejection was 68.2%, indicating TAC was not a worthy additive [57]. However, at 0.02 wt% TAC, the membrane water permeance was 3.10 LMH/bar and the NaCl rejection was 94.1%, indicating very low levels of TAC could be beneficial [57]. Increasing the TAC concentration led to polyamide membranes with a similar thickness, lower degree of cross-linking, higher hydrophilicity, and a multilayer-ring structure.

DMC is another co-solvent that has been used in heptane [82]. When DMC was used at a concentration of 1.5 wt%, the water permeance was the highest of the tested conditions at 4.52 LMH/bar and the NaCl rejection was 98.7% [82]. When DMC was used as a co-solvent, the resultant polyamide membrane was more leaf-like than nodule-like, rougher, and thicker.

Fig. 9 shows the water permeance and NaCl rejection data with outliers removed (see Supporting Information for details) for the organic co-solvents while keeping the MPD concentration, MPD soaking time, TMC concentration, and TMC reaction time constant. Statistical analyses (see Supporting Information for details) show that the polyamide membranes made with organic co-solvents had a statistically higher water permeance than the polyamide membrane made without organic co-solvents while the NaCl rejections were not significantly different from each other. Al-Hobaib et al. used EA and DEE in heptane at concentrations of 0–5 wt% [140]. It was found that EA at a concentration of 5 wt% produced membranes with a water permeance of 3.49 LMH/bar and a NaCl rejection of 97.0% [140]. DEE was found to work best at a concentration of 3 wt%, producing membranes with a water permeance of 2.72 LMH/bar and a NaCl rejection of 99.0% [140]. The addition of EA and DEE produced polyamide membranes which were slightly less rough and slightly more hydrophobic than membranes synthesized with no co-solvent [140]. Al-Hobaib et al. used EA, DEE, and acetone at concentrations of 0–3 wt% in both n-dodecane and n-hexane to produce polyamide membranes [148]. In n-hexane, EA at 3 wt%, DEE at 1 wt%, and acetone at 0.5 wt% provided the best results in terms of water permeance and NaCl rejection for each co-solvent [148]. The best performing membrane using n-hexane as the organic solvent was the EA at 3 wt% membrane, which had a water permeance of 2.75 LMH/bar and a NaCl rejection of 98.0% [148]. In n-dodecane, EA at 3 wt%, DEE at 1 wt %, and acetone at 0.5 wt% provided the best results in terms of water permeance and NaCl rejection [148]. Fig. 10 shows the best performing membrane using n-dodecane as the organic solvent was the EA at 3 wt% and DEE at 1 wt% membranes, which has a water permeance of 3.38 LMH/bar and a NaCl rejection of 97.0–98.0% [148]. The addition of EA, DEE, and acetone produced thicker polyamide membranes with a slightly lower roughness and higher hydrophobicity compared to membranes synthesized with no co-solvent [148]. Based on the discussed results, EA is a good additive to use in the organic phase (regardless of solvent) at concentrations of 3–5 wt% to improve the membrane permeance without sacrificing the NaCl rejection.

Tributyl phosphate (TBP) has been used in the organic phase as a complexing agent to reduce TMC reactivity [147,202]. It is challenging to deduce the direct effect TBP had on the resultant polyamide membrane due to TEA, CSA, EHD, and DMSO also being included as aqueous phase additives. However, when TBP was used in n-hexane, the resultant polyamide membrane was more hydrophilic than the polyamide membranes without the additives, and the polyamide membrane had a decrease in NaCl rejection to 87.8% and an increase in water permeance to 5.17 LMH/bar [147].

2.5. Processing techniques

2.5.1. Removal of aqueous amine solution techniques

In the process of fabricating thin-film composite polyamide membranes, a porous support membrane is first immersed in the aqueous amine solution, and after a given time, the excess aqueous MPD solution is removed from the top surface of the support membrane using one of several methods. The complete removal of the excess aqueous amine solution is critical as the presence of solution droplets on the membrane surface can form pinhole defects and reduce the salt rejection significantly [193]. Different methods have been used to remove the excess amine such as (1) using an air knife or air gun on the membrane surface [41,49,57,71,88,94,100,149], (2) applying compressed nitrogen on the membrane surface [23,54,60,78,90,103,106], or (3) using a roller on the membrane surface [22,40,43–48,50,51,53,55,58,59,61,64,65,68,70,77,79,81,83,86,87,92,97,101,102,105,112,113,115,119,120,124,125,131,136,137,141–144,146–148,150,152–154,156–159,161–164,203,204] until no extra solution droplets remain on the surface. The application of various methods can affect the lag time, which is defined as the time spent for eliminating the excess amine liquid from the top surface of the support until the amine-soaked support is exposed to the organic TMC solution. Lag time is considered to be an important factor in the synthesis process of TFC membranes, which affects the fabricated TFC membrane performance [205]. In the investigation performed by Fathizadeh et al., they found that increasing the lag time from 0 to 8 min caused a decrease in permeance from 0.95 LMH/bar to 0.14 LMH/bar [205]. However, regardless of lag time, any of the above-mentioned methods seem to be acceptable for removing the excess amine solution.

2.5.2. Post-reaction cross-linking techniques

Curing after the IP reaction assists cross-linking via additional reaction and increases the packing density, which results in the densification of the polyamide selective layer [194,206]. Some studies have suggested that the curing of the TFC membrane after the IP reaction has a significant impact on membrane performance [169,206]. Moreover, several studies have shown that curing is an important factor for stabilizing and strengthening the polyamide layer [207–209]. The curing of the polyamide layer via heat treatment increases the diffusivity of the MPD monomers, which increases the availability of MPD molecules in the reaction zone (and therefore increases the rate of reaction), enhances the rate of cross-linking, forms thick polyamide layers, and helps to shrink the pores of the substrate membrane, which enhances the salt rejection [169,177]. Some studies have investigated the curing time [194], other studies have investigated curing temperature [210], and others have investigated the curing medium [130]. Zargar et al. observed increased NaCl rejection and reduced water permeance when the curing time was increased from 10 to 20 min at 60 °C in an oven [194]. However, they were concerned about the fact that the longer curing time may destruct the polyamide layer due to the shrinkage of the polyamide layer, which will result in the formation of defects and a reduction in salt rejection [194,208]. When Dong et al. performed the post-reaction curing at 90 °C in an oven, they found that the water permeance was increased and NaCl rejection was decreased when increasing the curing time from 5 to 15 min [197]. They used TEA and CSA salt in the post-treatment solution, which helps the TFC membrane to withstand the heat treatment by protecting the reordering of the polyamide structure and avoiding the structural damage of the support membrane [197]. In another study, Ma et al. varied the post-curing temperature from 40 to 60 °C and found that by increasing the curing temperature in an oven, the NaCl rejection increased [210]. In other studies, different curing mediums have been applied in the post-reaction cross-linking process to investigate the effect of curing medium on the membrane performance [130,193]. The most common curing mediums are in an air-convection oven [37–41,43–48,50,52,53,55,59,61,66–68,73,80,85–88,93–96,111,116,120,121,123,129,131,133,134,136,138,139,142,143,145,152,159–162,165], a heated water bath [22,49,

65,71,130,164], air at room temperature [64,104,106,124,130], or steam [130], however numerous studies reported no post-reaction curing [23,42,51,54,56–58,60,62,63,69,70,72,74–79,81–84,89–92, 97–103,105,107–110,112–115,117–119,122,125–128,132,135,137, 140,141,144,146–151,153–158,163]. The most common oven curing temperature and time is 60 °C and 5 min. For instance, Xie et al. performed the post-reaction thermal treatment on the RO membrane using 80 °C for 10 min in an oven or 100 °C for 10 min in water [193]. The membranes cured in the oven showed higher water permeance (2.90 LMH/bar) compared to the water-cured membranes (2.45 LMH/bar) [193]. However, the NaCl rejection was almost the same for both membranes (99.2% for oven-cured and 99.5% for water-cured) [193]. Karimi et al. employed different curing mediums including air (8% relative humidity), steam (70% relative humidity), and deionized water for performing the post-curing reaction at 75 °C for 5 min [130]. They found that the polyamide RO membranes cured in the water had the highest NaCl rejection (99.7%), whereas the membrane cured in air showed the lowest NaCl rejection (98.3%) [130]. The water permeance for the steam-cured membrane (0.52 LMH/bar) was higher than the air-cured (0.46 LMH/bar) and water-cured (0.30 LMH/bar) membrane [130]. Membranes cured in air or steam were slightly more cross-linked than membranes cured in water. Membranes cured in air were less rough than membranes cured in steam or air. Membranes cured in water were more hydrophilic than membranes cured in steam, which were more hydrophilic than membranes cured in air.

Along with thermal curing, chemical post-treatments have a significant effect on membrane performance [32]. In order to improve the water permeability, several studies have focused on applying certain chemicals after interfacial polymerization [32,211,212]. In some studies, acids and bases have been employed for post-treatment [213,214]. For example, Kulkarni et al. applied hydrofluoric acid with a concentration below 5 wt% and observed an increase in the hydrophilicity, water permeance, and salt rejection [213]. Shen et al. found reduced salt rejection when they employed acids and bases during the post-treatment [214]. In the first step of the post-treatment process, they treated the TFC membrane with polyethyleneimine (PEI) [214]. In the second step, the authors further treated the PEI-modified membrane using an aqueous solution, where the pH was controlled in a range of 2 to 11 by varying the concentration of HCl and NaOH [214]. Among the PEI-modified membranes, the membrane which was treated in the most basic environment (pH = 11) was found to have the lowest salt rejection [214]. Due to the hydrolyzation of the amide group in the polyamide chain at the strong basic condition, the cross-linking density in the active layer was reduced and the salt rejection of the membrane was decreased [214]. Various solvents such as alcohols and other organics have been used for improving membrane performance [212,215]. For instance, when Idarraga-Mora et al. used short-chain (C_1–C_4) monohydric alcohols (specifically, methanol, ethanol, isopropyl alcohol, and 1-butanol) on commercial reverse osmosis membranes, they noticed a significant improvement in the water permeance [212]. Membranes contacted with methanol, ethanol, and 1-butanol had an increased surface roughness. It was suggested that an increase in free volume due to the disruption of inter-chain hydrogen bonds caused the improved permeance [212]. In another study, Mickols applied ethylenediamine and ethanolamine to the polyamide layer as the post-treatment step and observed that increasing the hydrogen bonding at the active layer can improve the surface hydrophilicity, which led to an increase in the water permeability of the membranes by 10% [216]. In another study, the application of benzyl alcohol improved the water permeance by 140% without compromising the salt rejection performance and decreased the surface roughness of the membranes [215]. In the work conducted by Kuehne et al., the water permeance of a synthesized polyamide membrane was found to be improved by 70% when they soaked the membrane in glycerol as the post-treatment step [211].

Redox initiation also has been used to improve RO membrane performance [217]. The fabricated RO membranes were immersed in a potassium persulfate solution which initiates the cross-linking reaction between the active layer and support layer and produced a thin polyamide layer with more functional groups and denser cross-linking [217]. The thin layer improved the water permeance and the denser cross-linking enhanced the salt rejection [217]. Membranes exposed to potassium persulfate had a lower surface roughness and higher hydrophilicity compared to membranes not exposed to potassium persulfate.

2.5.3. Storage medium

Once the polyamide membranes have been cured, the membranes are then stored in a solution until used or characterized. The most common storage solution is DI water [38,39,41,43–45,47,50–52,55,58, 59,63–66,70,72–74,76,78,80,83,85–89,91–98,100,101,106,107,110, 111,115,117–119,121,124,128,130,133–135,138,139,143,144,155, 158,161,164], however, some researchers store the membranes in DI water in a refrigerator at 4–5 °C [23,40,42,49,54,60,61,71,77,103, 104,125,131,132,137,140–142,148,150,165]. Storage in DI water is used to prevent pore collapse of the support and polyamide layers. Another storage solution used is aqueous 1.0 wt% sodium bisulfite ($NaHSO_3$) [37,57,67,105,114,116,123,127]. The $NaHSO_3$ is used to prevent bacteria growth in the storage water [105,123,127].

3. Characterization of polyamide layers

There are multiple ways RO polyamide layers have been characterized. Polyamide layer surface and cross-section morphology are often characterized by SEM, transmission electron microscopy (TEM), and AFM. Polyamide layer thickness has been determined through techniques such as AFM, SEM, TEM, ellipsometry, and other techniques to be discussed. The chemical composition of polyamide layers has been determined through techniques such as X-ray photoelectron spectroscopy (XPS), Fourier-transform infrared spectroscopy (FTIR), contact angle goniometry, and others to be discussed. The free volume and internal structure of polyamide layers are determined using PALS, TEM, and other techniques to be discussed. Mechanical properties of polyamide layers have been investigated using fracture strain and AFM nanoindentation techniques.

3.1. Surface and cross-sectional morphology

SEM (and field emission (FE)-SEM) is the most common method used to visualize the polyamide layer surface morphology and cross-section [22,23,37–61,63–165,167,172,177,179,181,193,201,218–227]. Most researchers rely on the cryo-cracking method to image the cross-section of polyamide membranes with [37,40,41,52,55,63,66,71,75,78,80, 83,105,110,134,138,139,146,150,151,159,162,163,172,193,224,225]. This method can be done in one of two ways. One method requires the polyester backing layer to be removed, then the polyamide + support layers are immersed in liquid nitrogen, followed by immediate fracturing upon removal from the liquid nitrogen. The second method requires immersing the whole membrane in liquid nitrogen, fracturing the polyamide + support layer, and then physically removing the backing layer. Another method to image the cross-section is what is called the “cryo-cutting” method [219,228]. This method does not require the removal of the polyester backing layer. Instead, the whole membrane and a razor blade are immersed in liquid nitrogen with both being held by a tool (such as a hemostat). Once the liquid nitrogen has stopped boiling, the membrane and razor blade are removed from the liquid nitrogen, and the razor blade is immediately used to slice the membrane. Careful attention must be made to not use a sawing motion with the razor blade as this will distort the membrane cross-section. Recently, as shown in Fig. 11, isolated polyamide layers, with the active side down, have been imaged by SEM to determine the number of pores and pore size on the backside (the side facing the support layer) of the polyamide layer [23,40,41,56,93,136,172,218].

Fig. 12 shows TEM is used to characterize the cross-sectional

morphology of polyamide layers [22,42,47,50,51,56,58,61,67,71,72,82,100,104,110,113,115,120,135,136,139,142,155,158,161,164,177,179,181,201,220,221,223–225,229,230]. In TEM, this is achieved by embedding the membrane in a resin and ultra-thin sections are cut using a microtome. In some instances, polyamide layers have been directly isolated on TEM grids to image the surface morphology of polyamide layers [40,41,53,56,68,123,134,161,164,172,179,222–224,230,231].

AFM in tapping mode is the most common method used to determine the surface roughness of dry polyamide layers [22,23,37–39,41,42,45–48,50,52–54,56,58–60,62–73,75–86,89–91,93,94,96,97,100–102,107,109,111–118,120,122,124,125,127,129,130,132–135,138–140,142,143,146–148,150,151,153,154,156–165,167,177,179,181,201,218,219,221,223,229–231]. Typical dry surface roughnesses are in the range of 90–190 nm [219,229]. Some researchers have imaged the surface roughness and morphology of wet membranes by performing AFM underwater [225]. Tip size and scanning speed are important variables to consider when performing AFM. If the tip size is too large, the tip will not measure the small features of the polyamide layer. This is one reason why profilometry is not commonly used for polyamide layer surface roughness [55]. If the scanning speed is too fast, then the tip will not have time to measure the surface features adequately. Laser measuring microscopy (LEXT) is a technique that can complement AFM to determine surface roughness [232]. However, if a surface is too rough, the laser will be too scattered to adequately calculate the polyamide surface roughness.

3.2. Thickness

Lin et al. characterized the thickness of six commercial polyamide layers by comparing SEM, TEM, AFM, Rutherford backscattering spectrometry (RBS), quartz crystal microbalance (QCM), profilometry, and ellipsometry techniques [220]. The authors found that AFM, RBS, QCM, profilometry, and ellipsometry had consistent results (90–200 nm for various commercial fully aromatic polyamide membranes) between the techniques, with ellipsometry being the most advantageous. However, this ellipsometry technique used by other researchers requires the cumbersome isolation of the polyamide layer, typically done on a silicon wafer [75,101,106,135,219,224,227,233]. Recently, Ogeiglo et al. demonstrated the use of ellipsometry without isolating the polyamide layer to determine the polyamide layer thickness [163,234].

SEM and TEM are common ways to determine the apparent polyamide layer thickness. In SEM, this is done by imaging the cross-section of the membrane [37–41,44,46,49,52–55,57,58,63,64,66,68,71,73,75,77,78,80,83,85–87,91,93,97,98,100,101,105,110–112,114,118,119,121,132,134,135,138,139,146,149–151,155,159,162,181,220,222]. In TEM, this is achieved by embedding the membrane in a resin and ultrathin sections are cut using a microtome [22,42,47,50,51,56,58,61,67,71,72,82,100,104,110,113,115,120,135,136,139,142,155,158,161,164,177,179,181,201,220–225,229,230]. Also, AFM is used to determine the polyamide layer thickness [37,93,181,220,224,227]. To use AFM, the polyamide layer is isolated on a silicon wafer, and the edge of or scratch in the polyamide layer is measured by the AFM tip to determine the thickness. Shaffer et al. used profilometry, a similar technique to AFM, to measure the polyamide layer thickness of their layer-by-layer grown films [235]. PALS can be used to estimate the polyamide layer thickness by probing the membrane free volume in the z-direction [110,236–239]. Where a large increase in free volume occurs indicates the interface of the active skin layer and the supporting layer. QCM and QCM-D (with dissipation) have been used to determine polyamide thicknesses produced from a layer-by-layer technique on silicon wafers [54,220,224,230]. QCM can determine the areal mass of the polyamide layer by analyzing the change in the frequency of the vibration from a bare QCM sensor and an isolated polyamide active layer on a QCM sensor.

3.3. Chemical composition

The chemical composition and properties of polyamide layers have been determined through numerous techniques. FTIR [23,43,67,69,73,80,81,85,86,111,112,128,132,135,151], and typically attenuated total reflectance (ATR)-FTIR [22,37,41,42,44,47,50–54,56–62,68,70,74–78,84,89,91–96,98,100,102,104–106,108,109,113–120,122,126,130,136,138–140,142,143,145–147,149,150,154,155,157,159,160,162,167,172,177,193,219,221,225,231,240], is commonly used to identify the chemical composition of polyamide layers. Some researchers have even isolated the polyamide layer for FTIR [23] and ATR-FTIR analysis [41,231]. Tang et al. have an excellent paper discussing the peaks associated with polysulfone, fully aromatic polyamide, and semi-aromatic polyamide membranes [240]. The key peaks for the fully aromatic polyamide layer are (1) ~1660 cm^{-1} representing the amide I band, (2) ~1610 cm^{-1} representing the aromatic amide, and (3) ~1540 cm^{-1} representing the amide II band [240]. A semi-aromatic polyamide layer (piperazine based) will only show the amide I band at ~1630 cm^{-1} [240]. Raman spectroscopy is a less common technique that is used to characterize the chemical structure polyamide membranes [64,98,124,133,136,160]. X-ray diffraction (XRD) also is sometimes used to characterize polyamide membranes [110,119,126,144], however, this is mostly done when comparing standard polyamide membranes with polyamide membranes containing nanoparticles.

XPS is commonly used to identify chemical composition and cross-linking density of polyamide layers [22,23,38,41,42,45,47,52,54,56,57,59,60,62,63,66,67,69,72–75,78,83–85,88–91,94–98,100,102,104,105,109,110,113–118,128–131,138,143,144,146,149,155,158–164,167,172,177,201,240,241]. The cross-linking density is determined by the nitrogen to oxygen (N/O) ratio using Eqs. (1) and (2), where m and n represent the cross-linked and linear part of the polyamide layer, respectively [161,177]. The N/O ratio can vary between 1, a fully cross-linked polyamide network where m = 1 and $n = 0$, and 0.5, a fully linear polyamide network where m = 0 and $n = 1$ [161]. Swelling ellipsometry experiments using the Painter-Shenoy equation are a good complement to XPS to determine the crosslinking density of the polyamide layer [219,234,242]. Also, energy dispersive X-ray spectroscopy (EDX) can be used to perform an elemental analysis of polyamide layers [43,44,49–52,63,65,70,73,80,92,125,131,134,137,141,147,148,152,181]. Silver ion binding experiments also have been used, sometimes paired with RBS experiments [243,244], to determine the carboxylic acid density of polyamide layers [219,245].

$$Crosslinking\ Density\ (\%) = \frac{m}{m+n} \times 100 \tag{1}$$

$$\frac{N}{O} = \frac{3m+2n}{3m+4n} \tag{2}$$

Membrane surface charge is characterized by zeta potential (also called streaming potential) measurements [22,39,42,45,53,55–57,59,60,62,64,66,67,75,78,81,84,85,89,94–96,98,100,101,106,108,112,113,117,120,122–124,127,132,133,135,145,146,162,163,201,221,225,229]. Fig. 13 shows this data obtained over a range of pHs, but it can also be obtained at a single pH. The data is then fit to either the Fairbrother-Mastin or Helmholtz-Smoluchowski equations. Uncoated fully aromatic polyamide membranes always show a negative surface charge at near-neutral pH due to the unreacted surface carboxylic acid groups present in the polyamide layer.

Contact angle goniometry often is used to characterize the hydrophilicity of polyamide layers [37–39,42–46,48,49,51–61,64–70,72–78,100–102,104–108,111–114,116–135,137,138,140–154,156–158,160,161,167,177,181,219,221,229]. Polyamide membranes contact angles are measured in the dry state using the sessile drop method or in the wet (swollen) state using the captive bubble method. Typical fully aromatic polyamide layers have sessile drop water contact angle values that range

from 40 to 100° [54,59,161,167,219,221,229]. However, contact angle measurements cannot fully describe the hydrophilicity of a polyamide surface because contact angle results are drastically affected by surface roughness and fully aromatic polyamide membranes are often very rough. The smooth fully aromatic polyamide membranes (~11 nm root mean square (RMS) roughness) made via 3D printing had a water contact angle of ~80° [181].

The thermal analysis of polyamide layers is challenging. Thermal gravimetric analysis (TGA) and differential scanning calorimetry (DSC) require a significant amount of the isolated polyamide layer to get adequate results, which is not practical. However, Ali et al. used DSC to show the effect of reaction time on T_g [165]. As the reaction time increased, the T_g increased [165]. To get around this, Maruf et al. used nano-thermal analysis (TA) to determine the T_g of polyamide layers [246,247]. Nano-TA utilizes a specialized AFM probe, which locally heats the polyamide surface in contact with the AFM probe. As the surface heats, thermal expansion of the surface occurs, and once the T_g is reached, the probe will penetrate the surface. Maruf et al. used this technique to show changes in T_g when the polyamide layers have been exposed to a chorine solution typically used for membrane cleaning [246,247].

3.4. Internal structure of polyamide layer

PALS is used to probe material defects, voids, and free volume at the sub-nanometer scale and, therefore, it is a useful tool for characterizing porous polyamide layers [166,236,239,248]. Other pore size analytical methods, such as BET (gas adsorption and desorption) and DSC, do not have enough sensitivity to quantify sub-nanometer holes [249]. PALS has been used to characterize the free volume of commercial and synthesized polyamide layers of NF and RO membranes [56,67,82,101,109,110,166,167,201,226,239,248,250–266]. The studies have found an average free-volume hole-radius of 0.2–0.29 nm [267]. Tuning of the free-volume hole-radius may be critical for fully aromatic polyamide membranes to adequately reject small, neutral molecules [267]. Molecular weight cut-off measurements of RO polyamide layers have been used to estimate pore size using various molecular weights of poly(ethylene glycol) (PEG), ethylene glycol, diethylene glycol, triethylene glycol, and sugars [81,162]. Wang et al. used small-angle X-ray scattering (SAXS) to quantify the polyamide layer pore size to be ~0.48 nm [93].

Lin et al. determined the polyamide layer pore volume using QCM measurements [224,230]. Some researchers have characterized the porous structure of polyamide membranes using SEM, TEM, and projection area (PA)-TEM [40,41,222,224]. Ogeiglo et al. used ellipsometry to approximate the polyamide layer average porosity (void volume fraction) and swelling in water and ethanol which is important for understanding molecular transport properties [234]. Lin et al. used ellipsometry, scanning transmission electron microscopy-energy dispersive X-ray spectroscopy (STEM-EDS), and scanning transmission electron microscopy-electron energy loss spectroscopy (STEM-EELS) to characterize the porous structure of polyamide membranes [224]. Kłosowski et al. used focused ion beam (FIB)-SEM and a combination of staining with STEM to estimate a 3D structure and permeation pathways of polyamide membranes [268]. Culp et al. used resonant soft X-ray scattering (RSoXS) and near-edge X-ray absorption fine structure (NEXAFS) spectra to correlate membrane structure and cross-linking density [231].

Recently, Chan et al. used small-angle neutron scattering (SANS) and quasi-elastic neutron scattering (QENS) to characterize the structure of and water transport mechanism in polyamide membranes [269]. They showed using QENS measurements that water diffuses through the polyamide layer at a rate similar to bulk water [269]. SANS revealed that the polyamide layer swelled relatively uniformly, but it did not swell enough to cause a significant change in length scale in the polyamide structure [269]. These results are confirmed by SANS measurements by Pipich et al. [226]. Culp et al. used electron tomography (HAADF-STEM) to render 3D morphologies of polyamide layers [270]. The authors claim that internal voids that are not open to the porous support layer make up $< 0.2\%$ of the total polymer volume [270]. This claim is two orders of magnitude less than what was previously reported by Pacheco et al. using TEM tomography [223].

3.5. Mechanical properties

The mechanical properties of polyamide layers are extremely challenging to measure due to the polyamide layer's thinness and fragility. A combined wrinkling-cracking method has been done to determine the polyamide layer elastic (Young's) modulus, strength, and fracture strain [271,272]. This technique, which requires the isolation of the polyamide layer, was used to detect embrittlement in polyamide layers after exposure to chlorine. The authors found the Young's modulus was 1.40 GPa, the fracture strength was 67 MPa, and the onset fracture strain was 14% for fully aromatic polyamide layers [272]. AFM nano-indentation experiments have been used on composite polyamide membranes to determine the Young's modulus of polyamide layers [219]. The authors found a commercial fully aromatic polyamide membrane had a Young's modulus of 2.7 GPa [219], slightly higher than what was found using the fracture strain method.

4. Hollow fiber fully aromatic polyamide membranes

There are only a few literature studies on hollow fiber (HF) fully aromatic membranes for RO. In most cases, the TFC layer is fabricated on the lumen or inner side of the HFs [273]. The challenge for RO HFs is to produce high NaCl rejecting membranes [273]. There are numerous studies on producing MPD-TMC polyamide layers on hollow fibers for water vapor permeation applications [274–278] and osmotic processes [279–285]. Khulbe and Matsuura recently reviewed strategies for TFC membranes for water treatment and other applications [273]. Gai et al. synthesized fully aromatic RO HF membranes using an aqueous solution containing 2 wt% MPD and 0.1 wt% SDS and a n-hexane solution containing 0.15 wt% TMC [286]. The produced HF membranes had a water permeance of 1.74 LMH/bar and a NaCl rejection of 98.2% [286]. The fabricated HF membranes had a similar surface structure and roughness as flat sheet membranes. Mondal and De synthesized fully aromatic NF HFs using an aqueous 2 wt% MPD solution and 0.1–1 wt% TMC in hexane solutions [287]. NaCl rejection was not reported, but the membrane made using 1.0 wt% TMC in hexane had a really low surface roughness of 4.3 nm, a water permeance of 4.10 LMH/bar and a molecular weight cut-off of 360 kDa [288]. Mohammadifakhr et al. produced polyamide RO HFs with at least 85% NaCl rejection by using a polyelectrolyte complex as an intermediate layer on the support HF [289]. The membranes produced using 2.5 wt% MPD in water and 0.15 wt% TMC in hexane had a water permeance of 0.3 LMH/bar [289]. Yabuno et al. synthesized RO HF membranes on the outside of the fibers by hydrolyzing a polyvinylidene difluoride (PVDF) or Psf support with poly(vinyl alcohol) (PVA) [290]. The polyamide synthesis was done with an aqueous solution containing 3 wt% MPD, 1.65 wt% TEA, 3.4 wt % CSA, 0.225 wt% SDS, and 1.5 wt% hexamethylphosphoric triamide and a hexane solution containing 0.15 wt% TMC [290]. When PVA was used the water permeance for membranes made on both supports was 2.26 LMH/bar and the NaCl rejection was 91.9% [290]. Without the PVA layer, the average membrane water permeance was 2.22 LMH/bar and the average NaCl rejection was 69.3% [290]. Lin et al. fabricated RO HF membranes on the inner side of the fiber using a 1.2 wt% MPD in water solution and a 0.1 wt% TMC in cyclohexane solution [291]. The produced HF membranes had a water permeance of 3.72 LMH/bar and a NaCl rejection of 96.5% [291]. Zhang et al. fabricated RO HF membranes on the inner side of the fibers using an aqueous solution containing 2 wt% MPD and 0.1 wt% SDS and a hexane solution containing 0.15 wt% TMC [292]. The produced HF membranes had a water

permeance of 7.39 LMH/bar and a NaCl rejection of 98.0% [292]. In an earlier work, Veríssimo et al. used a new technique to prepare RO HFs with the selective layer on the inner side [293]. Their technique used an inert liquid buffer of cyclohexane or FC-75 (a fluorinert liquid from 3M) between the aqueous MPD and the organic TMC solutions [293]. The produced membranes had a water permeance of 0.6 LMH/bar and a NaCl rejection of 99.5% [293].

5. Conclusions, recommendations, and future perspectives

In conclusion, there are numerous ways to synthesize fully aromatic polyamide RO membranes. While there is not one consistent way to synthesize a standard fully aromatic polyamide RO membrane, there is a common way RO membranes are synthesized based on the papers reviewed. The most common method is to immerse or contact a Psf membrane support in an aqueous 2 wt% MPD solution at room temperature for 2 min, remove the excess aqueous solution using a roller (often made of rubber), contact the MPD soaked membrane support with a 0.1 wt% TMC in n-hexane solution at room temperature for 1 min, remove the excess organic solution, cure in an oven at 60 °C for 5 min, rinse with copious amounts of water, and store in water until needed. The use of non-reactive additives and co-solvents can help improve membrane performance, if they are used in appropriate quantities. Ultimately, different labs synthesize RO membranes at the same conditions and get different results. Therefore, each lab has to determine what conditions work best for them. The characterization of RO polyamide layers is very standard in research labs across the world.

That being said, there is a need to understand why the same (or very similar) synthesis conditions can produce different results in different labs. More investigation into the interfacial polymerization kinetics on membrane supports could be beneficial to determining this answer. Determining the MPD concentration in the support membrane pores after excess aqueous solution removal and the diffusion rate and concentration of MPD in the organic solution from a MPD soaked membrane would provide further insight into the IP kinetics. The nano- and Angstrom scale characterization of polyamide layers also might provide further details into why this is the case. One important piece of information that is often missing in papers is the amount of MPD and TMC solutions used per membrane area. While the IP reaction is semi self-limiting, in order to adequately reproduce a membrane, all the details in the entire process must be known. Also, the reaction or solution temperature, even if at room temperature, needs to be reported more often to clarify the solution temperature at the start of the IP reaction. It would be very helpful to have a video accompanying the description of the synthesis to provide further clarification on the process used to synthesize the fully aromatic polyamide membranes. Many labs have successfully synthesized standard fully aromatic polyamide RO membranes, and thus, utilizing their expertise will be valuable for researchers learning to synthesize polyamide RO membranes.

CRediT authorship contribution statement

Shahriar Habib: Conceptualization, Data Curation, Formal Analysis, Writing - Original Draft, Writing – Review & Editing; **Steven T. Weinman**: Conceptualization, Data Curation, Formal Analysis, Writing - Original Draft, Writing – Review & Editing, Supervision, Project Administration, Funding Acquisition.

Declaration of competing interest

The authors declare that they have no known competing financial interests or personal relationships that could have appeared to influence the work reported in this paper.

Acknowledgments

The authors would like to acknowledge the financial support of the National Science Foundation (NSF) under grant number OIA-1928812 and to the Department of the Interior (DOI), Bureau of Reclamation (BR) under agreement number R19AC00087. Any opinions, findings, conclusions, and/or recommendations expressed in this material are those of the authors(s) and do not necessarily reflect the views of the NSF or the DOI, BR.

Abbreviations

AFM	atomic force microscopy
ATR	attenuated total reflectance
BHPF	9,9-bis(4-hydroxyphenyl) fluorene
CSA	(±)-camphor-10-sulfonic acid
DCM	dichloromethane
DEE	diethyl ether
DMC	dimethyl carbonate
DMSO	dimethyl sulfoxide
DSC	differential scanning calorimetry
EA	ethyl acetate
EDX	energy dispersive X-ray spectroscopy
EHD	2-ethyl-1,3-hexanediol
FE	field emission
FIB	focused ion beam
FTIR	Fourier-transform infrared spectroscopy
HF	hollow fiber
IP	interfacial polymerization
LCI	low coherence interferometry
LEXT	laser measuring microscopy
LMH/bar	$L/m^2/h/bar$
MF	microfiltration
MPD	m-phenylenediamine
NEXAFS	near-edge X-ray absorption fine structure
NF	nanofiltration
PA	projection area
PALS	positron annihilation lifetime spectroscopy
PC	polycarbonate
PEG	poly(ethylene glycol)
PEI	polyethyleimine
PES	polyethersulfone
PIP	piperazine
Psf	polysulfone
PVA	poly(vinyl alcohol)
PVDF	polyvinylidene difluoride
QCM	quartz crystal microbalance
QCM-D	quartz crystal microbalance with dissipation
RBS	Rutherford backscattering spectrometry
RES	resorcinol
RMS	root mean square
RO	reverse osmosis
RSoXS	resonant soft X-ray scattering
SAI	surface-averaged intensity
SANS	small-angle neutron scattering
SAXS	small-angle X-ray scattering
SDBS	sodium dodecylbenzenesulfonate
SDS	sodium dodecyl sulfate
SEM	scanning electron microscopy
SLS	sodium lauryl sulfate
STEM-EDS	scanning transmission electron microscopy-energy dispersive X-ray spectroscopy
STEM-EELS	scanning transmission electron microscopy-electron energy loss spectroscopy
TA	thermal analysis
TAC	trimellitic anhydride chloride

TBP	tributyl phosphate
TEA	triethylamine
TEM	transmission electron microscopy
TFC	thin-film composite
TGA	thermal gravimetric analysis
TMC	trimesoyl chloride
UF	ultrafiltration
XPS	X-ray photoelectron spectroscopy
XRD	X-ray diffraction

Appendix A. Supplementary data

Supplementary data to this article can be found online at https://doi.org/10.1016/j.desal.2021.114939.

References

[1] M.M. Mekonnen, A.Y. Hoekstra, Four billion people facing severe water scarcity, Sci. Adv. 2 (2016), e1500323.
[2] T. Veldkamp, Y. Wada, J. Aerts, P. Döll, S.N. Gosling, J. Liu, Y. Masaki, T. Oki, S. Ostberg, Y. Pokhrel, Water scarcity hotspots travel downstream due to human interventions in the 20th and 21st century, Nat. Commun. 8 (2017) 1–12.
[3] M. Kummu, J.H. Guillaume, H. de Moel, S. Eisner, M. Flörke, M. Porkka, S. Siebert, T.I. Veldkamp, P.J. Ward, The world's road to water scarcity: shortage and stress in the 20th century and pathways towards sustainability, Sci. Rep. 6 (2016) 38495.
[4] S.K. Patel, C.L. Ritt, A. Deshmukh, Z. Wang, M. Qin, R. Epsztein, M. Elimelech, The relative insignificance of advanced materials in enhancing the energy efficiency of desalination technologies, Energy Environ. Sci. 13 (2020) 1694–1710.
[5] M.R. Teixeira, M.J. Rosa, Comparing dissolved air flotation and conventional sedimentation to remove cyanobacterial cells of Microcystis aeruginosa: part II. The effect of water background organics, Sep. Purif. Technol. 53 (2007) 126–134.
[6] H.J. Tanudjaja, C.A. Hejase, V.V. Tarabara, A.G. Fane, J.W. Chew, Membrane-based separation for oily wastewater: a practical perspective, Water Res. 156 (2019) 347–365.
[7] L. Malaeb, G.M. Ayoub, Reverse osmosis technology for water treatment: state of the art review, Desalination 267 (2011) 1–8.
[8] J.R. Werber, S.K. Bull, M. Elimelech, Acyl-chloride quenching following interfacial polymerization to modulate the water permeability, selectivity, and surface charge of desalination membranes, J. Membr. Sci. 535 (2017) 357–364.
[9] C.E. Reid, E.J. Breton, Water and ion flow across cellulosic membranes, J. Appl. Polym. Sci. 1 (1959) 133–143.
[10] S. Loeb, S. Sourirajan, Sea Water Demineralization by Means of an Osmotic Membrane, in: Saline Water Conversion—II, AMERICAN CHEMICAL SOCIETY, 1963, pp. 117–132.
[11] M.C. Porter, What, when, and why of membranes-MF, UF and RO, AIChE Symp. Ser. 73 (1977) 83–103.
[12] H.K. Lonsdale, Reverse osmosis, in: P.M. Bungay, H.K. Lonsdale, M.N. de Pinho (Eds.), Synthetic Membranes: Science, Engineering and Applications, Springer Netherlands, Dordrecht, 1986, pp. 307–342.
[13] J.K. Beasley, The evaluation and selection of polymeric materials for reverse osmosis membranes, Desalination 22 (1977) 181–189.
[14] J.W. Richter, H.H. Hoehn, Permselective, Aromatic, Nitrogen-Containing Polymeric Membranes, in, Google Patents, 1971.
[15] J.E. Cadotte, Interfacially synthesized reverse osmosis membrane, in: T.U.S.P.a.T. Office (Ed.), Filmtec Corp. (Patent Application No. 4277344A), United States, 1981.
[16] K.P. Lee, T.C. Arnot, D. Mattia, A review of reverse osmosis membrane materials for desalination—development to date and future potential, J. Membr. Sci. 370 (2011) 1–22.
[17] Z. Yang, Y. Zhou, Z. Feng, X. Rui, T. Zhang, Z. Zhang, A Review on Reverse Osmosis and Nanofiltration Membranes for Water Purification, Polymers, 11 (2019).
[18] A. Al Mayyahi, Important Approaches to Enhance Reverse Osmosis (RO) Thin Film Composite (TFC) Membranes Performance, Membranes, 8 (2018).
[19] M. Qasim, M. Badrelzaman, N.N. Darwish, N.A. Darwish, N. Hilal, Reverse osmosis desalination: a state-of-the-art review, Desalination 459 (2019) 59–104.
[20] G.-R. Xu, J.-M. Xu, H.-J. Feng, H.-L. Zhao, S.-B. Wu, Tailoring structures and performance of polyamide thin film composite (PA-TFC) desalination membranes via sublayers adjustment-a review, Desalination 417 (2017) 19–35.
[21] M. Aghajani, A.R. Greenberg, Y. Ding, Thin film composite membranes: does the porous support truly have negligible resistance? J. Membr. Sci. 609 (2020) 118207.
[22] L.E. Peng, Z. Yao, X. Liu, B. Deng, H. Guo, C.Y. Tang, Tailoring polyamide rejection layer with aqueous carbonate chemistry for enhanced membrane separation: mechanistic insights, chemistry-structure-property relationship, and environmental implications, Environmental Science & Technology 53 (2019) 9764–9770.
[23] J. Wang, R. Xu, F. Yang, J. Kang, Y. Cao, M. Xiang, Probing influences of support layer on the morphology of polyamide selective layer of thin film composite membrane, J. Membr. Sci. 556 (2018) 374–383.
[24] J.-A.-D. Sharabati, S. Guclu, S. Erkoc-Ilter, D.Y. Koseoglu-Imer, S. Unal, Y. Z. Menceloglu, I. Ozturk, I. Koyuncu, Interfacially polymerized thin-film composite membranes: impact of support layer pore size on active layer polymerization and seawater desalination performance, Sep. Purif. Technol. 212 (2019) 438–448.
[25] Q. Zhang, Z. Zhang, L. Dai, H. Wang, S. Li, S. Zhang, Novel insights into the interplay between support and active layer in the thin film composite polyamide membranes, J. Membr. Sci. 537 (2017) 372–383.
[26] A.K. Ghosh, E.M.V. Hoek, Impacts of support membrane structure and chemistry on polyamide–polysulfone interfacial composite membranes, J. Membr. Sci. 336 (2009) 140–148.
[27] H. Saleem, L. Trabzon, A. Kilic, S.J. Zaidi, Recent advances in nanofibrous membranes: production and applications in water treatment and desalination, Desalination 478 (2020) 114178.
[28] Q. Liu, G.-R. Xu, Graphene oxide (GO) as functional material in tailoring polyamide thin film composite (PA-TFC) reverse osmosis (RO) membranes, Desalination 394 (2016) 162–175.
[29] A. Giwa, N. Akther, V. Dufour, S.W. Hasan, A critical review on recent polymeric and nano-enhanced membranes for reverse osmosis, RSC Adv. 6 (2016) 8134–8163.
[30] B. Antrim, R. Lesan, B. Liu, A. von Gottberg, Worlds largest spiral element — history and development, Desalination 178 (2005) 313–324.
[31] C. Bartels, M. Hirose, H. Fujioka, Performance advancement in the spiral wound RO/NF element design, Desalination 221 (2008) 207–214.
[32] A. Al Mayyahi, Important approaches to enhance reverse osmosis (RO) thin film composite (TFC) membranes performance, Membranes 8 (2018) 68.
[33] Z. Yang, H. Guo, C.Y. Tang, The upper bound of thin-film composite (TFC) polyamide membranes for desalination, J. Membr. Sci. 590 (2019) 117297.
[34] J.R. Werber, A. Deshmukh, M. Elimelech, The critical need for increased selectivity, not increased water permeability, for desalination membranes, Environmental Science & Technology Letters 3 (2016) 112–120.
[35] T. Matsuura, Progress in membrane science and technology for seawater desalination — a review, Desalination 134 (2001) 47–54.
[36] M. Hirose, H. Ito, Y. Kamiyama, Effect of skin layer surface structures on the flux behaviour of RO membranes, J. Membr. Sci. 121 (1996) 209–215.
[37] H. Wu, X. Zhang, X.-T. Zhao, K. Li, C.-Y. Yu, L.-F. Liu, Y.-F. Zhou, C.-J. Gao, High flux reverse osmosis membranes fabricated with hyperbranched polymers via novel twice-crosslinked interfacial polymerization method, J. Membr. Sci. 595 (2020) 117480.
[38] Q. Zhao, D.L. Zhao, T.-S. Chung, Nanoclays-incorporated thin-film nanocomposite membranes for reverse osmosis desalination, Adv. Mater. Interfaces 7 (2020) 1902108.
[39] H. Zhang, Y. Wang, Y. Wei, C. Gao, G. Zhu, Fabrication of polyamide thin film nanocomposite reverse osmosis membrane incorporated with a novel graphite-based carbon material for desalination, J. Appl. Polym. Sci. 137 (2020) 49030.
[40] H. Yan, X. Miao, J. Xu, G. Pan, Y. Zhang, Y. Shi, M. Guo, Y. Liu, The porous structure of the fully-aromatic polyamide film in reverse osmosis membranes, J. Membr. Sci. 475 (2015) 504–510.
[41] Z. Zhang, Y. Qin, G. Kang, H. Yu, Y. Jin, Y. Cao, Tailoring the internal void structure of polyamide films to achieve highly permeable reverse osmosis membranes for water desalination, J. Membr. Sci. 595 (2020) 117518.
[42] R. Xu, L. Ding, D. Chen, T. Liu, Y. Wu, Y. Cao, J. Chen, F. Yang, J. Kang, M. Xiang, Enhancing the chlorine stability and antifouling properties of thin-film composite reverse osmosis membranes via surface grafting L-arginine-functionalized polyvinyl alcohol, Ind. Eng. Chem. Res. 59 (2020) 10882–10893.
[43] H. Marioryad, A.M. Ghaedi, D. Emadzadeh, M.M. Baneshi, A. Vafaei, W.-J. Lau, A thin film nanocomposite reverse osmosis membrane incorporated with S-beta zeolite nanoparticles for water desalination, ChemistrySelect 5 (2020) 1972–1975.
[44] S. Feng, Z.-X. Low, S. Liu, L. Zhang, X. Zhang, G.P. Simon, X.-Y. Fang, H. Wang, Microporous polymer incorporated polyamide membrane for reverse osmosis desalination, J. Membr. Sci. 610 (2020) 118299.
[45] G. Zhang, J. Zhang, P. Lv, J. Sun, P. Zhao, L. Yang, Modifying thin film composite membrane with zeolitic imidazolate framework-8@polydopamine for enhanced antifouling property, Chemosphere 248 (2020) 125956.
[46] S. Seyyed Shahabi, N. Azizi, V. Vatanpour, Tuning thin-film composite reverse osmosis membranes using deep eutectic solvents and ionic liquids toward enhanced water permeation, J. Membr. Sci. 610 (2020) 118267.
[47] P. Karami, B. Khorshidi, J.B.P. Soares, M. Sadrzadeh, Fabrication of highly permeable and thermally stable reverse osmosis thin film composite polyamide membranes, ACS Appl. Mater. Interfaces 12 (2020) 2916–2925.
[48] V. Vatanpour, M. Safarpour, A. Khataee, H. Zarrabi, M.E. Yekavalangi, M. Kavian, A thin film nanocomposite reverse osmosis membrane containing amine-functionalized carbon nanotubes, Sep. Purif. Technol. 184 (2017) 135–143.
[49] M. Di Vincenzo, M. Barboiu, A. Tiraferri, Y.M. Legrand, Polyol-functionalized thin-film composite membranes with improved transport properties and boron removal in reverse osmosis, J. Membr. Sci. 540 (2017) 71–77.
[50] Z. Yang, X. Huang, X.-h. Ma, Z.-w. Zhou, H. Guo, Z. Yao, S.-P. Feng, C.Y. Tang, Fabrication of a novel and green thin-film composite membrane containing nanovoids for water purification, J. Membr. Sci. 570-571 (2019) 314–321.
[51] A.A. Mayyahi, Thin-film composite (TFC) membrane modified by hybrid ZnO-graphene nanoparticles (ZnO-Gr NPs) for water desalination, Journal of Environmental Chemical Engineering 6 (2018) 1109–1117.

[52] B. Rodríguez, D. Oztürk, M. Rosales, M. Flores, A. García, Antibiofouling thin-film composite membranes (TFC) by in situ formation of Cu-(m-phenylenediamine) oligomer complex, J. Mater. Sci. 53 (2018) 6325–6338.
[53] X. Tian, J. Wang, H. Zhang, Z. Cao, M. Zhao, Y. Guan, Y. Zhang, Establishment of transport channels with carriers for water in reverse osmosis membrane by incorporating hydrotalcite into the polyamide layer, RSC Adv. 8 (2018) 12439–12448.
[54] X. Song, S. Qi, C.Y. Tang, C. Gao, Ultra-thin, multi-layered polyamide membranes: synthesis and characterization, J. Membr. Sci. 540 (2017) 10–18.
[55] Y. Manawi, V. Kochkodan, A.F. Ismail, A.W. Mohammad, M. Ali Atieh, Performance of acacia gum as a novel additive in thin film composite polyamide RO membranes, Membranes 9 (2019) 30.
[56] Y. Liu, W. Yan, Z. Wang, H. Wang, S. Zhao, J. Wang, P. Zhang, X. Cao, 1-methylimidazole as a novel additive for reverse osmosis membrane with high flux-rejection combinations and good stability, J. Membr. Sci. 599 (2020) 117830.
[57] Z. Zhang, G. Kang, H. Yu, Y. Jin, Y. Cao, From reverse osmosis to nanofiltration: precise control of the pore size and charge of polyamide membranes via interfacial polymerization, Desalination 466 (2019) 16–23.
[58] X. Hu, J. Sun, R. Peng, Q. Tang, Y. Luo, P. Yu, Novel thin-film composite reverse osmosis membrane with superior water flux using parallel magnetic field induced magnetic multi-walled carbon nanotubes, J. Clean. Prod. 242 (2020) 118423.
[59] S.-L. Li, P. Wu, J. Wang, J. Wang, Y. Hu, Fabrication of high performance polyamide reverse osmosis membrane from monomer 4-morpholino-m-phenylenediamine and tailoring with zwitterions, Desalination 473 (2020) 114169.
[60] T. Liu, D. Chen, F. Yang, J. Chen, Y. Cao, M. Xiang, J. Kang, R. Xu, Enhancing the permeability and anti-fouling properties of a polyamide thin-film composite reverse osmosis membrane via surface grafting of l-lysine, RSC Adv. 9 (2019) 20044–20052.
[61] M. Kadhom, B. Deng, Thin film nanocomposite membranes filled with bentonite nanoparticles for brackish water desalination: a novel water uptake concept, Microporous Mesoporous Mater. 279 (2019) 82–91.
[62] M. Abdulsalam Ebrahim, S. Karan, A.G. Livingston, On the influence of salt concentration on the transport properties of reverse osmosis membranes in high pressure and high recovery desalination, J. Membr. Sci. 594 (2020) 117339.
[63] K. Zarshenas, G. Jiang, J. Zhang, M.A. Jauhar, Z. Chen, Atomic scale manipulation of sublayer with functional TiO2 nanofilm toward high-performance reverse osmosis membrane, Desalination 480 (2020) 114342.
[64] H.-R. Chae, J. Lee, C.-H. Lee, I.-C. Kim, P.-K. Park, Graphene oxide-embedded thin-film composite reverse osmosis membrane with high flux, anti-biofouling, and chlorine resistance, J. Membr. Sci. 483 (2015) 128–135.
[65] M.-P. Li, X. Zhang, H. Zhang, W.-L. Liu, Z.-H. Huang, F. Xie, X.-H. Ma, Z.-L. Xu, Hydrophilic yolk-shell ZIF-8 modified polyamide thin-film nanocomposite membrane with improved permeability and selectivity, Sep. Purif. Technol. 247 (2020) 116990.
[66] S. Zhang, Q.V. Ly, L.D. Nghiem, J. Wang, J. Li, Y. Hu, Optimization and organic fouling behavior of zwitterion-modified thin-film composite polyamide membrane for water reclamation: a comprehensive study, J. Membr. Sci. 596 (2020) 117748.
[67] R.-H. Li, Y. Li, H. Wu, W.-T. Yan, C.-Y. Yu, L.-F. Liu, C.-J. Gao, Structure regulation for synergistically improving the permeation properties of the reverse osmosis membrane based on an amphiphilic hyperbranched polymer, J. Membr. Sci. 608 (2020) 118143.
[68] X. Tian, Z. Cao, J. Wang, J. Chen, Y. Wei, Development of high-performance mixed matrix reverse osmosis membranes by incorporating aminosilane-modified hydrotalcite, RSC Adv. 10 (2020) 5648–5655.
[69] X. Wang, Q. Li, J. Zhang, H. Huang, S. Wu, Y. Yang, Novel thin-film reverse osmosis membrane with MXene Ti3C2Tx embedded in polyamide to enhance the water flux, anti-fouling and chlorine resistance for water desalination, J. Membr. Sci. 603 (2020) 118036.
[70] M. Asadollahi, D. Bastani, S.A. Mousavi, H. Heydari, D.V. Mousavi, Improvement of performance and fouling resistance of polyamide reverse osmosis membranes using acrylamide and TiO2 nanoparticles under UV irradiation for water desalination, J. Appl. Polym. Sci. 137 (2020) 48461.
[71] D.M. Davenport, C.L. Ritt, R. Verbeke, M. Dickmann, W. Egger, I.F. J. Vankelecom, M. Elimelech, Thin film composite membrane compaction in high-pressure reverse osmosis, Journal of Membrane Science (2020) 118268.
[72] B.L. Bonnett, E.D. Smith, M. De La Garza, M. Cai, J.V. Haag, J.M. Serrano, H. D. Cornell, B. Gibbons, S.M. Martin, A.J. Morris, PCN-222 metal–organic framework nanoparticles with tunable pore size for nanocomposite reverse osmosis membranes, ACS Appl. Mater. Interfaces 12 (2020) 15765–15773.
[73] N. Li, L. Yu, Z. Xiao, C. Jiang, B. Gao, Z. Wang, Biofouling mitigation effect of thin film nanocomposite membranes immobilized with laponite mediated metal ions, Desalination 473 (2020) 114162.
[74] S.R. Khairkar, A.V. Pansare, A.A. Shedge, S.Y. Chhatre, A.K. Suresh, S. Chakrabarti, V.R. Patil, A.A. Nagarkar, Hydrophobic interpenetrating polyamide-PDMS membranes for desalination, pesticides removal and enhanced chlorine tolerance, Chemosphere 258 (2020) 127179.
[75] Z. Ali, B.S. Ghanem, Y. Wang, F. Pacheco, W. Ogieglo, H. Vovusha, G. Genduso, U. Schwingenschlögl, Y. Han, I. Pinnau, Finely tuned submicroporous thin-film molecular sieve membranes for highly efficient fluid separations, Adv. Mater. 32 (2020) 2001132.
[76] F. Jahangiri, M. Asadollahi, S.A. Mousavi, F. Farhadi, Improvement of performance of polyamide reverse osmosis membranes using dielectric barrier discharge plasma treatment as a novel surface modification method, Polym. Eng. Sci. 59 (2019) E468–E475.
[77] M. Fathizadeh, H.N. Tien, K. Khivantsev, Z. Song, F. Zhou, M. Yu, Polyamide/nitrogen-doped graphene oxide quantum dots (N-GOQD) thin film nanocomposite reverse osmosis membranes for high flux desalination, Desalination 451 (2019) 125–132.
[78] D. Chen, Q. Chen, T. Liu, J. Kang, R. Xu, Y. Cao, M. Xiang, Influence of l-arginine on performances of polyamide thin-film composite reverse osmosis membranes, RSC Adv. 9 (2019) 20149–20160.
[79] S.T. Iranizadeh, M.P. Chenar, M.N. Mahboub, H.A. Namaghi, Preparation and characterization of thin-film composite reverse osmosis membrane on a novel aminosilane-modified polyvinyl chloride support, Braz. J. Chem. Eng. 36 (2019) 251–264.
[80] H. Sun, D. Li, B. Liu, J. Yao, Enhancing the permeability of TFC membranes based on incorporating polyamide matrix into MWCNTs framework, Appl. Surf. Sci. 496 (2019) 143680.
[81] Y. Yao, W. Zhang, Y. Du, M. Li, L. Wang, X. Zhang, Toward enhancing the chlorine resistance of reverse osmosis membranes: an effective strategy via an end-capping technology, Environmental Science & Technology 53 (2019) 1296–1304.
[82] M. Shi, W. Yan, Y. Zhou, Z. Wang, L. Liu, S. Zhao, Y. Ji, J. Wang, C. Gao, P. Zhang, X. Cao, Combining tannic acid-modified support and a green co-solvent for high performance reverse osmosis membranes, J. Membr. Sci. 595 (2020) 117474.
[83] T.H. Lee, J.Y. Oh, S.P. Hong, J.M. Lee, S.M. Roh, S.H. Kim, H.B. Park, ZIF-8 particle size effects on reverse osmosis performance of polyamide thin-film nanocomposite membranes: importance of particle deposition, J. Membr. Sci. 570-571 (2019) 23–33.
[84] X. Zhang, H. Huang, Q. Li, H. Yu, X. Tian, M. Zhao, H. Zhang, Facile dual-functionalization of polyamide reverse osmosis membrane by a natural polypeptide to improve the antifouling and chlorine-resistant properties, J. Membr. Sci. 604 (2020) 118044.
[85] Y. Liu, C. Liu, X. Fu, O. Lin, Z. Wang, C. Wang, C. Zhang, Armor polyamide reverse osmosis membrane with POSS 'armors' through two-step interfacial polymerization for high anti-chlorine and anti-bacteria performance, J. Membr. Sci. 586 (2019) 211–221.
[86] T.C. Yu, Z.A. Karim, W.T. Whye, Water transport properties of boron nitride nanosheets incorporated thin film nanocomposite membrane for salt removal, Malaysian Journal of Fundamental and Applied Sciences 15 (2019) 790–794.
[87] A. Ismail, R.M. Tajuddin, H. Mohktar, A.F. Ismail, Effect of Kenaf MCC Composition on Thin Film Composite Membrane for NaCI Rejection, in: MATEC Web of Conferences, EDP Sciences, 2019.
[88] C. Xu, F. Shao, Z. Yi, H. Dong, Q. Zhang, J. Yu, J. Feng, X. Wu, Q. Zhang, L. Yu, L. Dong, Highly chlorine resistance polyamide reverse osmosis membranes with oxidized graphitic carbon nitride by ontology doping method, Sep. Purif. Technol. 223 (2019) 178–185.
[89] Y. Zhang, Y. Wan, M. Guo, G. Pan, H. Shi, X. Yao, Y. Liu, Surface modification on thin-film composite reverse osmosis membrane by cation complexation for antifouling, J. Polym. Res. 26 (2019) 68.
[90] F. Wang, T. Zheng, R. Xiong, P. Wang, J. Ma, Strong improvement of reverse osmosis polyamide membrane performance by addition of ZIF-8 nanoparticles: effect of particle size and dispersion in selective layer, Chemosphere 233 (2019) 524–531.
[91] C. Liu, Y. Guo, J. Zhang, B. Tian, O. Lin, Y. Liu, C. Zhang, Tailor-made high-performance reverse osmosis membranes by surface fixation of hydrophilic macromolecules for wastewater treatment, RSC Adv. 9 (2019) 17766–17777.
[92] Z.C. Ng, C.Y. Chong, W.J. Lau, M. Karaman, A.F. Ismail, Boron removal and antifouling properties of thin-film nanocomposite membrane incorporating PECVD-modified titanate nanotubes, J. Chem. Technol. Biotechnol. 94 (2019) 2772–2782.
[93] S. Wang, K. Gu, J. Wang, Y. Zhou, C. Gao, Enhanced the swelling resistance of polyamide membranes with reinforced concrete structure, J. Membr. Sci. 575 (2019) 191–199.
[94] Y. Zhang, Y. Wan, G. Pan, X. Wei, Y. Li, H. Shi, Y. Liu, Preparation of high performance polyamide membrane by surface modification method for desalination, J. Membr. Sci. 573 (2019) 11–20.
[95] Y. Zhao, L. Dai, Q. Zhang, S. Zhang, Surface modification of polyamide reverses osmosis membrane by phosphonic acid group with improved performance, J. Appl. Polym. Sci. 136 (2019) 46931.
[96] S. Wang, Y. Zhou, C. Gao, Novel high boron removal polyamide reverse osmosis membranes, J. Membr. Sci. 554 (2018) 244–252.
[97] T.H. Lee, I. Park, J.Y. Oh, J.K. Jang, H.B. Park, Facile preparation of polyamide thin-film nanocomposite membranes using spray-assisted nanofiller predeposition, Ind. Eng. Chem. Res. 58 (2019) 4248–4256.
[98] C. Liu, C. Wang, Y. Guo, J. Zhang, Y. Cao, H. Liu, Z. Hu, C. Zhang, High-performance polyamide membrane with tailored water channel prepared via bionic neural networks for textile wastewater treatment, J. Mater. Chem. A 7 (2019) 6695–6707.
[99] A.M.A. Abdelsamad, M. Matthias, A.S.G. Khalil, M. Ulbricht, Nanofillers dissolution as a crucial challenge for the performance stability of thin-film nanocomposite desalination membranes, Sep. Purif. Technol. 228 (2019) 115767.
[100] R. Xu, G. Xu, J. Wang, J. Chen, F. Yang, J. Kang, M. Xiang, Influence of l-lysine on the permeation and antifouling performance of polyamide thin film composite reverse osmosis membranes, RSC Adv. 8 (2018) 25236–25247.
[101] Y. Yao, M. Li, X. Cao, P. Zhang, W. Zhang, J. Zheng, X. Zhang, L. Wang, A novel sulfonated reverse osmosis membrane for seawater desalination: experimental and molecular dynamics studies, J. Membr. Sci. 550 (2018) 470–479.

[102] L.-Y. Chen, L.-P. Wu, H.-L. Zhang, Y.-B. Gao, J.-G. Gai, Tris(hydroxymethyl) aminomethane polyamide thin-film-composite antifouling reverse osmosis membrane, J. Appl. Polym. Sci. 135 (2018) 45891.
[103] Y. He, H. Hoi, S. Abraham, C.D. Montemagno, Highly permeable biomimetic reverse osmosis membrane with amphiphilic peptide stabilized aquaporin as water filtering agent, J. Appl. Polym. Sci. 135 (2018) 46169.
[104] S. Cao, G. Zhang, C. Xiong, S. Long, X. Wang, J. Yang, Preparation and characterization of thin-film-composite reverse-osmosis polyamide membrane with enhanced chlorine resistance by introducing thioether units into polyamide layer, J. Membr. Sci. 564 (2018) 473–482.
[105] S. Gholami, A. Rezvani, V. Vatanpour, J.L. Cortina, Improving the chlorine resistance property of polyamide TFC RO membrane by polyethylene glycol diacrylate (PEGDA) coating, Desalination 443 (2018) 245–255.
[106] E. Maaskant, W. Vogel, T.J. Dingemans, N.E. Benes, The use of a star-shaped trifunctional acyl chloride for the preparation of polyamide thin film composite membranes, J. Membr. Sci. 567 (2018) 321–328.
[107] A. Al Mayyahi, TiO2 polyamide thin film nanocomposite reverses osmosis membrane for water desalination, Membranes 8 (2018) 66.
[108] R. Mehta, P. Bharda, S. Sharma, A. Bhattacharya, Mitigation of arsenic from water through tailor-made thin film composite (TFC) membrane, MOJ Polymer Science 2 (2018), 00042.
[109] J. Ortiz-Medina, S. Inukai, T. Araki, A. Morelos-Gomez, R. Cruz-Silva, K. Takeuchi, T. Noguchi, T. Kawaguchi, M. Terrones, M. Endo, Robust water desalination membranes against degradation using high loads of carbon nanotubes, Sci. Rep. 8 (2018) 2748.
[110] C. Van Goethem, R. Verbeke, M. Pfanmöller, T. Koschine, M. Dickmann, T. Timpel-Lindner, W. Egger, S. Bals, I.F.J. Vankelecom, The role of MOFs in thin-film nanocomposite (TFN) membranes, J. Membr. Sci. 563 (2018) 938–948.
[111] S. Al Aani, A. Haroutounian, C.J. Wright, N. Hilal, Thin film nanocomposite (TFN) membranes modified with polydopamine coated metals/carbon-nanostructures for desalination applications, Desalination 427 (2018) 60–74.
[112] S. Lin, Y. Li, L. Zhang, S. Chen, L.a. Hou, Zwitterion-like, Charge-Balanced Ultrathin Layers on Polymeric Membranes for Antifouling Property, Environmental Science & Technology, 52 (2018) 4457–4463.
[113] J.-E. Gu, S. Lee, C.M. Stafford, J.S. Lee, W. Choi, B.-Y. Kim, K.-Y. Baek, E.P. Chan, J.Y. Chung, J. Bang, J.-H. Lee, Molecular layer-by-layer assembled thin-film composite membranes for water desalination, Adv. Mater. 25 (2013) 4778–4782.
[114] M. Yam-Cervantes, Y. Pérez-Padilla, M. Aguilar-Vega, TFC reverse osmosis polyamide membranes—effect of increasing sulfonic group concentration on water flux and salt rejection performance, J. Appl. Polym. Sci. 135 (2018) 46500.
[115] H.M. Park, K.Y. Jee, Y.T. Lee, Preparation and characterization of a thin-film composite reverse osmosis membrane using a polysulfone membrane including metal-organic frameworks, J. Membr. Sci. 541 (2017) 510–518.
[116] H. Wu, X.-L. Chen, X. Huang, H.-M. Ruan, Y.-L. Ji, L.-F. Liu, C.-J. Gao, A novel semi-aromatic polyamide TFC reverse osmosis membrane fabricated from a dendritic molecule of trimesoylamidoamine through a two-step amine-immersion mode, RSC Adv. 7 (2017) 39127–39137.
[117] Y. Zhang, Y. Wan, G. Pan, H. Shi, H. Yan, J. Xu, M. Guo, Z. Wang, Y. Liu, Surface modification of polyamide reverse osmosis membrane with sulfonated polyvinyl alcohol for antifouling, Appl. Surf. Sci. 419 (2017) 177–187.
[118] Y. Zhang, X. Miao, G. Pan, H. Shi, H. Yan, J. Xu, M. Guo, S. Li, Y. Zhang, Y. Liu, Highly improved permeation property of thin-film-composite polyamide membrane for water desalination, J. Polym. Res. 24 (2016) 5.
[119] Y.H. Kotp, Y.A. Shebl, M.S. El-Deab, B.E. El-Anadouli, H.A. Shawky, Performance enhancement of PA-TFC RO membrane by using magnesium silicate nanoparticles, J. Inorg. Organomet. Polym. Mater. 27 (2017) 201–214.
[120] Y. Baek, H.J. Kim, S.-H. Kim, J.-C. Lee, J. Yoon, Evaluation of carbon nanotube-polyamide thin-film nanocomposite reverse osmosis membrane: surface properties, performance characteristics and fouling behavior, J. Ind. Eng. Chem. 56 (2017) 327–334.
[121] J. Farahbakhsh, M. Delnavaz, V. Vatanpour, Investigation of raw and oxidized multiwalled carbon nanotubes in fabrication of reverse osmosis polyamide membranes for improvement in desalination and antifouling properties, Desalination 410 (2017) 1–9.
[122] T. Zhang, K. Zhang, J. Li, X. Yue, Simultaneously enhancing hydrophilicity, chlorine resistance and anti-biofouling of APA-TFC membrane surface by densely grafting quaternary ammonium cations and salicylaldimines, J. Membr. Sci. 528 (2017) 296–302.
[123] M. Zhao, H.F. Zhang, H. Huang, Y.S. Zhang, Preparation and Properties of Nanocomposite MWCNTs/Polyamide Reverse Osmosis Membrane for Desalination by Interfacial Polymerization, in: Key Engineering Materials, Trans Tech Publications, Ltd, 2017, pp. 1016–1025.
[124] H.-R. Chae, C.-H. Lee, P.-K. Park, I.-C. Kim, J.-H. Kim, Synergetic effect of graphene oxide nanosheets embedded in the active and support layers on the performance of thin-film composite membranes, J. Membr. Sci. 525 (2017) 99–106.
[125] J. Ghoul, I. Ghiloufi, L. Mir, S. Arabia, Efficiency of polyamide thin-film nanocomposite membrane containing ZnO nanoparticles, Journal of Ovonic Research Vol 13 (2017) 83–90.
[126] Y.A. Shebl, Y.H. Kotp, H.A. Shawky, M.S. El-Deab, B.E. El-Anadouli, Enhancement of PA-TFC RO Membrane by Using Inorganic Nanoparticles, in: Twentieth International Water Technology Conference, Hurghada, Egpyt, 2017, pp. 597–614.
[127] M. Zhao, S. Fu, H. Zhang, H. Huang, Y. Wei, Y. Zhang, Enhanced separation and antifouling performance of reverse osmosis membrane incorporated with carbon nanotubes functionalized by atom transfer radical polymerization, RSC Adv. 7 (2017) 46969–46979.
[128] F. Shao, C. Xu, W. Ji, H. Dong, Q. Sun, L. Yu, L. Dong, Layer-by-layer self-assembly TiO2 and graphene oxide on polyamide reverse osmosis membranes with improved membrane durability, Desalination 423 (2017) 21–29.
[129] R. Pang, K. Zhang, High-flux polyamide reverse osmosis membranes by surface grafting 4-(2-hydroxyethyl)morpholine, RSC Adv. 7 (2017) 40705–40710.
[130] H. Karimi, M. Bazrgar Bajestani, S.A. Mousavi, R. Mokhtari Garakani, Polyamide membrane surface and bulk modification using humid environment as a new heat curing medium, J. Membr. Sci. 523 (2017) 129–137.
[131] M. Zargar, Y. Hartanto, B. Jin, S. Dai, Polyethylenimine modified silica nanoparticles enhance interfacial interactions and desalination performance of thin film nanocomposite membranes, J. Membr. Sci. 541 (2017) 19–28.
[132] I.M.A. ElSherbiny, A.S.G. Khalil, M. Ulbricht, Surface micro-patterning as a promising platform towards novel polyamide thin-film composite membranes of superior performance, J. Membr. Sci. 529 (2017) 11–22.
[133] R. Pang, K. Zhang, A facile and viable approach to fabricate polyamide membranes functionalized with graphene oxide nanosheets, RSC Adv. 7 (2017) 53463–53471.
[134] L. Liu, G. Zhu, Z. Liu, C. Gao, Effect of MCM-48 nanoparticles on the performance of thin film nanocomposite membranes for reverse osmosis application, Desalination 394 (2016) 72–82.
[135] J. Hu, Y. Pu, M. Ueda, X. Zhang, L. Wang, Charge-aggregate induced (CAI) reverse osmosis membrane for seawater desalination and boron removal, J. Membr. Sci. 520 (2016) 1–7.
[136] H.J. Kim, Y.-S. Choi, M.-Y. Lim, K.H. Jung, D.-G. Kim, J.-J. Kim, H. Kang, J.-C. Lee, Reverse osmosis nanocomposite membranes containing graphene oxides coated by tannic acid with chlorine-tolerant and antimicrobial properties, J. Membr. Sci. 514 (2016) 25–34.
[137] A.S. Al-Hobaib, J. El Ghoul, I. Ghiloufi, L. El Mir, Synthesis and characterization of polyamide thin-film nanocomposite membrane reached by aluminum doped ZnO nanoparticles, Mater. Sci. Semicond. Process. 42 (2016) 111–114.
[138] Y. Xu, X. Gao, X. Wang, Q. Wang, Z. Ji, X. Wang, T. Wu, C. Gao, Highly and stably water permeable thin film nanocomposite membranes doped with MIL-101 (Cr) nanoparticles for reverse osmosis application, Materials 9 (2016) 870.
[139] S.H. Maruf, A.R. Greenberg, Y. Ding, Influence of substrate processing and interfacial polymerization conditions on the surface topography and permselective properties of surface-patterned thin-film composite membranes, J. Membr. Sci. 512 (2016) 50–60.
[140] A. Al-Hobaib, M. Alsuhybani, K.M. Al-Sheetan, M.R. Shaik, Reverse osmosis membranes prepared by interfacial polymerization in n-heptane containing different co-solvents, Desalin. Water Treat. 57 (2016) 16733–16744.
[141] A.S. Al-Hobaib, K.M. Al-Sheetan, L. El Mir, Effect of iron oxide nanoparticles on the performance of polyamide membrane for ground water purification, Mater. Sci. Semicond. Process. 42 (2016) 107–110.
[142] J. Yin, G. Zhu, B. Deng, Graphene oxide (GO) enhanced polyamide (PA) thin-film nanocomposite (TFN) membrane for water purification, Desalination 379 (2016) 93–101.
[143] S. Lin, H. Huang, Y. Zeng, L. Zhang, L.a. Hou, Facile surface modification by aldehydes to enhance chlorine resistance of polyamide thin film composite membranes, Journal of Membrane Science, 518 (2016) 40–49.
[144] M.E.A. Ali, F.M. Hassan, X. Feng, Improving the performance of TFC membranes via chelation and surface reaction: applications in water desalination, J. Mater. Chem. A 4 (2016) 6620–6629.
[145] T. Zhang, X. Yue, C. Zhu, H. Ma, Y. Liu, J. Li, B. Pan, Densely grafting quaternary ammonium cation and salicylaldehyde on the APA-TFC membrane surface for enhancing chlorine resistance and anti-biofouling properties, Desalin. Water Treat. 57 (2016) 16384–16394.
[146] H. Hoseinpour, M. Peyravi, A. Nozad, M. Jahanshahi, Static and dynamic assessments of polysulfonamide and poly(amide-sulfonamide) acid-stable membranes, J. Taiwan Inst. Chem. Eng. 67 (2016) 453–466.
[147] S.J. Kim, P.S. Lee, S. Bano, Y.I. Park, S.E. Nam, K.H. Lee, Effective incorporation of TiO2 nanoparticles into polyamide thin-film composite membranes, Journal of Applied Polymer Science, 133 (2016).
[148] A.S. Al-Hobaib, M.S. Al-Suhybani, K.M. Al-Sheetan, H. Mousa, M.R. Shaik, New RO TFC membranes by interfacial polymerization in n-dodecane with various co-solvents, Membranes 6 (2016) 24.
[149] S.-H. Park, Y.-S. Ko, S.-J. Park, J.S. Lee, J. Cho, K.-Y. Baek, I.T. Kim, K. Woo, J.-H. Lee, Immobilization of silver nanoparticle-decorated silica particles on polyamide thin film composite membranes for antibacterial properties, J. Membr. Sci. 499 (2016) 80–91.
[150] W.-F. Chan, E. Marand, S.M. Martin, Novel zwitterion functionalized carbon nanotube nanocomposite membranes for improved RO performance and surface anti-biofouling resistance, J. Membr. Sci. 509 (2016) 125–137.
[151] L. Wang, S. Duan, M. Fang, J. Liu, J. He, J. Li, J. Lei, Surface modification route to prepare novel polyamide@NH2_MIL-88B nanocomposite membranes for water treatment, RSC Adv. 6 (2016) 71250–71261.
[152] J. Kim, Y. Baek, S.P. Hong, H. Yoon, S. Kim, C. Kim, J. Kim, J. Yoon, Evaluation of thin-film nanocomposite RO membranes using TiO2 nanotubes and TiO2 nanoparticles: a comparative study, Desalin. Water Treat. 57 (2016) 24674–24681.
[153] F. Wu, X. Liu, C. Au, Effects of DMSO and glycerol additives on the property of polyamide reverse osmosis membrane, Water Sci. Technol. 74 (2016) 1619–1625.
[154] F. Jahangiri, S.A. Mousavi, F. Farhadi, V. Vatanpour, B. Sabzi, Z. Chenari, Effect of CO 2-laser irradiation on properties and performance of thin-film composite

polyamide reverse osmosis membrane, Korean J. Chem. Eng. 33 (2016) 1028–1036.
[155] C. Van Goethem, R. Verbeke, S. Hermans, R. Bernstein, I.F. Vankelecom, Controlled positioning of MOFs in interfacially polymerized thin-film nanocomposites, J. Mater. Chem. A 4 (2016) 16368–16376.
[156] M. Safarpour, A. Khataee, V. Vatanpour, Thin film nanocomposite reverse osmosis membrane modified by reduced graphene oxide/TiO2 with improved desalination performance, J. Membr. Sci. 489 (2015) 43–54.
[157] A. Bera, R.M. Gol, S. Chatterjee, S.K. Jewrajka, PEGylation and incorporation of triazine ring into thin film composite reverse osmosis membranes for enhancement of anti-organic and anti-biofouling properties, Desalination 360 (2015) 108–117.
[158] J. Duan, E. Litwiller, I. Pinnau, Preparation and water desalination properties of POSS-polyamide nanocomposite reverse osmosis membranes, J. Membr. Sci. 473 (2015) 157–164.
[159] Y.J. Lim, J. Lee, T.-H. Bae, J. Torres, R. Wang, Feasibility and performance of a thin-film composite seawater reverse osmosis membrane fabricated on a highly porous microstructured support, J. Membr. Sci. 611 (2020) 118407.
[160] C. Liu, J. Zhang, W. Wang, Y. Guo, K. Xiao, Effects of gamma-ray irradiation on separation and mechanical properties of polyamide reverse osmosis membrane, J. Membr. Sci. 611 (2020) 118354.
[161] B. Khorshidi, T. Thundat, D. Pernitsky, M. Sadrzadeh, A parametric study on the synergistic impacts of chemical additives on permeation properties of thin film composite polyamide membrane, J. Membr. Sci. 535 (2017) 248–257.
[162] J. Lee, R. Wang, T.-H. Bae, A comprehensive understanding of co-solvent effects on interfacial polymerization: interaction with trimesoyl chloride, J. Membr. Sci. 583 (2019) 70–80.
[163] Z. Ali, Y. Al Sunbul, F. Pacheco, W. Ogieglo, Y. Wang, G. Genduso, I. Pinnau, Defect-free highly selective polyamide thin-film composite membranes for desalination and boron removal, J. Membr. Sci. 578 (2019) 85–94.
[164] X.-H. Ma, Z.-K. Yao, Z. Yang, H. Guo, Z.-L. Xu, C.Y. Tang, M. Elimelech, Nanofoaming of polyamide desalination membranes to tune permeability and selectivity, Environmental Science & Technology Letters 5 (2018) 123–130.
[165] F.A.A. Ali, J. Alam, A.K. Shukla, M. Alhoshan, B.M.A. Abdo, W.A. Al-Masry, A novel approach to optimize the fabrication conditions of thin film composite RO membranes using multi-objective genetic algorithm II, Polymers 12 (2020) 494.
[166] S.H. Kim, S.-Y. Kwak, T. Suzuki, Positron annihilation spectroscopic evidence to demonstrate the flux-enhancement mechanism in morphology-controlled thin-film-composite (TFC) membrane, Environmental Science & Technology 39 (2005) 1764–1770.
[167] L. Shen, W.-s. Hung, J. Zuo, X. Zhang, J.-Y. Lai, Y. Wang, High-performance thin-film composite polyamide membranes developed with green ultrasound-assisted interfacial polymerization, J. Membr. Sci. 570-571 (2019) 112–119.
[168] M. Dalwani, N.E. Benes, G. Bargeman, D. Stamatialis, M. Wessling, Effect of pH on the performance of polyamide/polyacrylonitrile based thin film composite membranes, J. Membr. Sci. 372 (2011) 228–238.
[169] A.K. Ghosh, B.-H. Jeong, X. Huang, E.M.V. Hoek, Impacts of reaction and curing conditions on polyamide composite reverse osmosis membrane properties, J. Membr. Sci. 311 (2008) 34–45.
[170] T. Fujioka, B.E. O'Rourke, K. Michishio, Y. Kobayashi, N. Oshima, H. Kodamatani, T. Shintani, L.D. Nghiem, Transport of small and neutral solutes through reverse osmosis membranes: role of skin layer conformation of the polyamide film, J. Membr. Sci. 554 (2018) 301–308.
[171] H. An, J.W. Smith, W. Chen, Z. Ou, Q. Chen, Charting the quantitative relationship between two-dimensional morphology parameters of polyamide membranes and synthesis conditions, Molecular Systems Design & Engineering 5 (2020) 102–109.
[172] J. Xu, H. Yan, Y. Zhang, G. Pan, Y. Liu, The morphology of fully-aromatic polyamide separation layer and its relationship with separation performance of TFC membranes, J. Membr. Sci. 541 (2017) 174–188.
[173] M.F. Jimenez-Solomon, Q. Song, K.E. Jelfs, M. Munoz-Ibanez, A.G. Livingston, Polymer nanofilms with enhanced microporosity by interfacial polymerization, Nat. Mater. 15 (2016) 760–767.
[174] H.B. Park, J. Kamcev, L.M. Robeson, M. Elimelech, B.D. Freeman, Maximizing the right stuff: The trade-off between membrane permeability and selectivity, Science, 356 (2017) eaab0530.
[175] C. Kong, M. Kanezashi, T. Yamomoto, T. Shintani, T. Tsuru, Controlled synthesis of high performance polyamide membrane with thin dense layer for water desalination, J. Membr. Sci. 362 (2010) 76–80.
[176] W.J. Lau, A.F. Ismail, N. Misdan, M.A. Kassim, A recent progress in thin film composite membrane: a review, Desalination 287 (2012) 190–199.
[177] B. Khorshidi, T. Thundat, B.A. Fleck, M. Sadrzadeh, A novel approach toward fabrication of high performance thin film composite polyamide membranes, Sci. Rep. 6 (2016) 22069.
[178] F. Pacheco, 3D visualization of the internal nanostructure of polyamide thin films in RO membranes, Journal of membrane science, v. 501 (2016) pp. 12-44-2016 v.2501.
[179] X. Ma, Z. Yang, Z. Yao, H. Guo, Z. Xu, C.Y. Tang, Tuning roughness features of thin film composite polyamide membranes for simultaneously enhanced permeability, selectivity and anti-fouling performance, J. Colloid Interface Sci. 540 (2019) 382–388.
[180] T.J. Mason, Ultrasound in synthetic organic chemistry, Chem. Soc. Rev. 26 (1997) 443–451.
[181] M.R. Chowdhury, J. Steffes, B.D. Huey, J.R. McCutcheon, 3D printed polyamide membranes for desalination, Science 361 (2018) 682.
[182] A. Nowbahar, V. Mansard, J.M. Mecca, M. Paul, T. Arrowood, T.M. Squires, Measuring interfacial polymerization kinetics using microfluidic interferometry, J. Am. Chem. Soc. 140 (2018) 3173–3176.
[183] D. Ren, J.I.N. Yeo, T.-Y. Liu, X. Wang, Time-dependent FTIR microscopy for mechanism investigations and kinetic measurements in interfacial polymerisation: a microporous polymer film study, Polym. Chem. 10 (2019) 2769–2773.
[184] W. Li, X. Liu, Z. Li, A.G. Fane, B. Deng, Unraveling the film-formation kinetics of interfacial polymerization via low coherence interferometry, AICHE J. 66 (2020), e16863.
[185] S. Behera, S.K. Akkihebbal, Intrinsic kinetics of interfacial polycondensation reactions– the reaction of mPDA with TMC, Polymer 210 (2020) 122982.
[186] S. Behera, A.K. Suresh, Kinetics of interfacial hydrolysis of an aromatic acid chloride, Chem. Eng. Res. Des. 146 (2019) 154–161.
[187] S. Behera, A.K. Suresh, Data on of interfacial hydrolysis kinetics of an aromatic acid chloride, Data in Brief 26 (2019) 104337.
[188] S. Behera, A.K. Suresh, Kinetics of interfacial polycondensation reactions – development of a new method and its validation, Polymer 127 (2017) 28–44.
[189] L.E. Peng, Z. Yao, Z. Yang, H. Guo, C.Y. Tang, Dissecting the role of substrate on the morphology and separation properties of thin film composite polyamide membranes: seeing is believing, Environmental Science & Technology 54 (2020) 6978–6986.
[190] B. Khorshidi, T. Thundat, B. Fleck, M. Sadrzadeh, Thin film composite polyamide membranes: parametric study on the influence of synthesis conditions, RSC Adv. 5 (2015) 54985–54997.
[191] G.-Y. Chai, W.B. Krantz, Formation and characterization of polyamide membranes via interfacial polymerization, J. Membr. Sci. 93 (1994) 175–192.
[192] I.J. Roh, A.R. Greenberg, V.P. Khare, Synthesis and characterization of interfacially polymerized polyamide thin films, Desalination 191 (2006) 279–290.
[193] W. Xie, G.M. Geise, B.D. Freeman, H.-S. Lee, G. Byun, J.E. McGrath, Polyamide interfacial composite membranes prepared from m-phenylene diamine, trimesoyl chloride and a new disulfonated diamine, J. Membr. Sci. 403 (2012) 152–161.
[194] M. Zargar, B. Jin, S. Dai, An integrated statistic and systematic approach to study correlation of synthesis condition and desalination performance of thin film composite membranes, Desalination 394 (2016) 138–147.
[195] V. Vatanpour, M. Sheydaei, M. Esmaeili, Box-Behnken design as a systematic approach to inspect correlation between synthesis conditions and desalination performance of TFC RO membranes, Desalination 420 (2017) 1–11.
[196] M. Kadhom, B. Deng, Synthesis of high-performance thin film composite (TFC) membranes by controlling the preparation conditions: technical notes, Journal of Water Process Engineering 30 (2019) 100542.
[197] H. Dong, L. Zhao, L. Zhang, H. Chen, C. Gao, W.S. Winston Ho, High-flux reverse osmosis membranes incorporated with NaY zeolite nanoparticles for brackish water desalination, J. Membr. Sci. 476 (2015) 373–383.
[198] B. Ukrainsky, G.Z. Ramon, Temperature measurement of the reaction zone during polyamide film formation by interfacial polymerization, J. Membr. Sci. 566 (2018) 329–335.
[199] J.M. Gohil, P. Ray, A review on semi-aromatic polyamide TFC membranes prepared by interfacial polymerization: potential for water treatment and desalination, Sep. Purif. Technol. 181 (2017) 159–182.
[200] S.H. Maruf, A.R. Greenberg, J. Pellegrino, Y. Ding, Fabrication and characterization of a surface-patterned thin film composite membrane, J. Membr. Sci. 452 (2014) 11–19.
[201] Y. Liang, Y. Zhu, C. Liu, K.-R. Lee, W.-S. Hung, Z. Wang, Y. Li, M. Elimelech, J. Jin, S. Lin, Polyamide nanofiltration membrane with highly uniform sub-nanometre pores for sub-1 Å precision separation, Nat. Commun. 11 (2020) 2015.
[202] I.-C. Kim, B.-R. Jeong, S.-J. Kim, K.-H. Lee, Preparation of high flux thin film composite polyamide membrane: the effect of alkyl phosphate additives during interfacial polymerization, Desalination 308 (2013) 111–114.
[203] Y.A. Shebl, Y.H. Kotp, H.A. Shawky, M.S. El-Deab, B.E. El-Anadouli, ENHANCEMENT OF PA-TFC RO MEMBRANE BY USING INORGANIC NANOPARTICLES.
[204] F.A.A. Ali, J. Alam, A.K. Shukla, M. Alhoshan, B.M.A. Abdo, W.A. Al-Masry, A novel approach to optimize the fabrication conditions of thin film composite RO membranes using multi-objective genetic algorithm II, Polymers 12 (2020) 494.
[205] M. Fathizadeh, A. Aroujalian, A. Raisi, Effect of lag time in interfacial polymerization on polyamide composite membrane with different hydrophilic sub layers, Desalination 284 (2012) 32–41.
[206] T.A. Otitoju, R.A. Saari, A.L. Ahmad, Progress in the modification of reverse osmosis (RO) membranes for enhanced performance, J. Ind. Eng. Chem. 67 (2018) 52–71.
[207] F.T. Minhas, S. Memon, M.I. Bhanger, N. Iqbal, M. Mujahid, Solvent resistant thin film composite nanofiltration membrane: characterization and permeation study, Appl. Surf. Sci. 282 (2013) 887–897.
[208] R.-X. Zhang, J. Vanneste, L. Poelmans, A. Sotto, X.-L. Wang, B. Van der Bruggen, Effect of the manufacturing conditions on the structure and performance of thin-film composite membranes, J. Appl. Polym. Sci. 125 (2012) 3755–3769.
[209] A. Prakash Rao, N.V. Desai, R. Rangarajan, Interfacially synthesized thin film composite RO membranes for seawater desalination, J. Membr. Sci. 124 (1997) 263–272.
[210] R. Ma, Y.-L. Ji, X.-D. Weng, Q.-F. An, C.-J. Gao, High-flux and fouling-resistant reverse osmosis membrane prepared with incorporating zwitterionic amine monomers via interfacial polymerization, Desalination 381 (2016) 100–110.
[211] M.A. Kuehne, R.Q. Song, N.N. Li, R.J. Petersen, Flux enhancement in TFC RO membranes, Environ. Prog. 20 (2001) 23–26.

[212] J.A. Idarraga-Mora, M.A. Lemelin, S.T. Weinman, S.M. Husson, Effect of short-term contact with C1–C4 monohydric alcohols on the water permeance of MPD-TMC thin-film composite reverse osmosis membranes, Membranes 9 (2019) 92.
[213] A. Kulkarni, D. Mukherjee, W.N. Gill, Flux enhancement by hydrophilization of thin film composite reverse osmosis membranes, J. Membr. Sci. 114 (1996) 39–50.
[214] L. Shen, X. Zhang, J. Zuo, Y. Wang, Performance enhancement of TFC FO membranes with polyethyleneimine modification and post-treatment, J. Membr. Sci. 534 (2017) 46–58.
[215] M.G. Shin, S.-H. Park, S.J. Kwon, H.-E. Kwon, J.B. Park, J.-H. Lee, Facile performance enhancement of reverse osmosis membranes via solvent activation with benzyl alcohol, J. Membr. Sci. 578 (2019) 220–229.
[216] W.E. Mickols, Method of treating polyamide membranes to increase flux, in, Google Patents, 1998.
[217] S. Bing, J. Wang, H. Xu, Y. Zhao, Y. Zhou, L. Zhang, C. Gao, L.a. Hou, Polyamide thin-film composite membrane modified with persulfate for improvement of perm-selectivity and chlorine-resistance, Journal of Membrane Science, 555 (2018) 318–326.
[218] X. Song, B. Gan, Z. Yang, C.Y. Tang, C. Gao, Confined nanobubbles shape the surface roughness structures of thin film composite polyamide desalination membranes, J. Membr. Sci. 582 (2019) 342–349.
[219] S.T. Weinman, E.M. Fierce, S.M. Husson, Nanopatterning commercial nanofiltration and reverse osmosis membranes, Sep. Purif. Technol. 209 (2019) 646–657.
[220] L. Lin, C. Feng, R. Lopez, O. Coronell, Identifying facile and accurate methods to measure the thickness of the active layers of thin-film composite membranes – a comparison of seven characterization techniques, J. Membr. Sci. 498 (2016) 167–179.
[221] X.-H. Ma, Z. Yang, Z.-K. Yao, H. Guo, Z.-L. Xu, C.Y. Tang, Interfacial polymerization with electrosprayed microdroplets: toward controllable and ultrathin polyamide membranes, Environmental Science & Technology Letters 5 (2018) 117–122.
[222] F.A. Pacheco, I. Pinnau, M. Reinhard, J.O. Leckie, Characterization of isolated polyamide thin films of RO and NF membranes using novel TEM techniques, J. Membr. Sci. 358 (2010) 51–59.
[223] F. Pacheco, R. Sougrat, M. Reinhard, J.O. Leckie, I. Pinnau, 3D visualization of the internal nanostructure of polyamide thin films in RO membranes, J. Membr. Sci. 501 (2016) 33–44.
[224] L. Lin, R. Lopez, G.Z. Ramon, O. Coronell, Investigating the void structure of the polyamide active layers of thin-film composite membranes, J. Membr. Sci. 497 (2016) 365–376.
[225] S. Hermans, R. Bernstein, A. Volodin, I.F.J. Vankelecom, Study of synthesis parameters and active layer morphology of interfacially polymerized polyamide–polysulfone membranes, React. Funct. Polym. 86 (2015) 199–208.
[226] V. Pipich, K. Schlenstedt, M. Dickmann, R. Kasher, J. Meier-Haack, C. Hugenschmidt, W. Petry, Y. Oren, D. Schwahn, Morphology and porous structure of standalone aromatic polyamide films as used in RO membranes – an exploration with SANS, PALS, and SEM, Journal of Membrane Science 573 (2019) 167–176.
[227] J.M. Dennison, X. Xie, C.J. Murphy, D.G. Cahill, Density, Elastic Constants, and Thermal Conductivity of Interfacially Polymerized Polyamide Films for Reverse Osmosis Membranes, ACS Applied Nano Materials, 1 (2018) 5008–5018.
[228] L. Huang, N.-N. Bui, M.T. Meyering, T.J. Hamlin, J.R. McCutcheon, Novel hydrophilic nylon 6,6 microfiltration membrane supported thin film composite membranes for engineered osmosis, J. Membr. Sci. 437 (2013) 141–149.
[229] C.Y. Tang, Y.-N. Kwon, J.O. Leckie, Effect of membrane chemistry and coating layer on physiochemical properties of thin film composite polyamide RO and NF membranes: II. Membrane physiochemical properties and their dependence on polyamide and coating layers, Desalination 242 (2009) 168–182.
[230] L. Lin, T.M. Weigand, M.W. Farthing, P. Jutaporn, C.T. Miller, O. Coronell, Relative importance of geometrical and intrinsic water transport properties of active layers in the water permeability of polyamide thin-film composite membranes, J. Membr. Sci. 564 (2018) 935–944.
[231] T.E. Culp, D. Ye, M. Paul, A. Roy, M.J. Behr, S. Jons, S. Rosenberg, C. Wang, E. W. Gomez, M. Kumar, E.D. Gomez, Probing the internal microstructure of polyamide thin-film composite membranes using resonant soft X-ray scattering, ACS Macro Lett. 7 (2018) 927–932.
[232] S.T. Weinman, S.M. Husson, Influence of chemical coating combined with nanopatterning on alginate fouling during nanofiltration, J. Membr. Sci. 513 (2016) 146–154.
[233] K. Kezia, J. Lee, W. Ogieglo, A. Hill, N.E. Benes, S.E. Kentish, The transport of hydronium and hydroxide ions through reverse osmosis membranes, J. Membr. Sci. 459 (2014) 197–206.
[234] W. Ogieglo, J.A. Idarraga-Mora, S.M. Husson, I. Pinnau, Direct ellipsometry for non-destructive characterization of interfacially-polymerized thin-film composite membranes, J. Membr. Sci. 608 (2020) 118174.
[235] D.L. Shaffer, K.E. Feldman, E.P. Chan, G.R. Stafford, C.M. Stafford, Characterizing salt permeability in polyamide desalination membranes using electrochemical impedance spectroscopy, J. Membr. Sci. 583 (2019) 248–257.
[236] H. Chen, W.-S. Hung, C.-H. Lo, S.-H. Huang, M.-L. Cheng, G. Liu, K.-R. Lee, J.-Y. Lai, Y.-M. Sun, C.-C. Hu, R. Suzuki, T. Ohdaira, N. Oshima, Y.C. Jean, Free-volume depth profile of polymeric membranes studied by positron annihilation spectroscopy: layer structure from interfacial polymerization, Macromolecules 40 (2007) 7542–7557.
[237] W.-S. Hung, M. De Guzman, S.-H. Huang, K.-R. Lee, Y.C. Jean, J.-Y. Lai, Characterizing free volumes and layer structures in asymmetric thin-film polymeric membranes in the wet condition using the variable monoenergy slow positron beam, Macromolecules 43 (2010) 6127–6134.
[238] H. Hagihara, K. Ito, N. Oshima, A. Yabuuchi, H. Suda, H. Yanagishita, Depth profiling of the free-volume holes in cellulose triacetate hollow-fiber membranes for reverse osmosis by means of variable-energy positron annihilation lifetime spectroscopy, Desalination 344 (2014) 86–89.
[239] D.W. Gidley, H.-G. Peng, R.S. Vallery, Positron annihilation as a method to characterize porous materials, Annu. Rev. Mater. Res. 36 (2006) 49–79.
[240] C.Y. Tang, Y.-N. Kwon, J.O. Leckie, Effect of membrane chemistry and coating layer on physiochemical properties of thin film composite polyamide RO and NF membranes: I. FTIR and XPS characterization of polyamide and coating layer chemistry, Desalination 242 (2009) 149–167.
[241] C. Buechner, S.M. Gericke, L. Trotochaud, O. Karslıoğlu, J. Raso, H. Bluhm, Quantitative characterization of a desalination membrane model system by X-ray photoelectron spectroscopy, Langmuir 35 (2019) 11315–11321.
[242] E.P. Chan, A.P. Young, J.-H. Lee, C.M. Stafford, Swelling of ultrathin molecular layer-by-layer polyamide water desalination membranes, J. Polym. Sci. B Polym. Phys. 51 (2013) 1647–1655.
[243] O. Coronell, B.J. Mariñas, D.G. Cahill, Depth heterogeneity of fully aromatic polyamide active layers in reverse osmosis and nanofiltration membranes, Environmental Science & Technology 45 (2011) 4513–4520.
[244] O. Coronell, B.J. Mariñas, X. Zhang, D.G. Cahill, Quantification of functional groups and modeling of their ionization behavior in the active layer of FT30 reverse osmosis membrane, Environmental Science & Technology 42 (2008) 5260–5266.
[245] D. Chen, J.R. Werber, X. Zhao, M. Elimelech, A facile method to quantify the carboxyl group areal density in the active layer of polyamide thin-film composite membranes, J. Membr. Sci. 534 (2017) 100–108.
[246] S.H. Maruf, D.U. Ahn, J. Pellegrino, J.P. Killgore, A.R. Greenberg, Y. Ding, Correlation between barrier layer Tg and a thin-film composite polyamide membrane's performance: effect of chlorine treatment, J. Membr. Sci. 405 (2012) 167–175.
[247] S.H. Maruf, D.U. Ahn, A.R. Greenberg, Y. Ding, Glass transition behaviors of interfacially polymerized polyamide barrier layers on thin film composite membranes via nano-thermal analysis, Polymer 52 (2011) 2643–2649.
[248] T.C. Merkel, B.D. Freeman, R.J. Spontak, Z. He, I. Pinnau, P. Meakin, A.J. Hill, Ultrapermeable, Reverse-Selective Nanocomposite Membranes, Science, 296 (2002) 519–522.
[249] Y.C. Jean, J.D. Van Horn, W.-S. Hung, K.-R. Lee, Perspective of positron annihilation spectroscopy in polymers, Macromolecules 46 (2013) 7133–7145.
[250] K. Boussu, J. De Baerdemaeker, C. Dauwe, M. Weber, K.G. Lynn, D. Depla, S. Aldea, I.F.J. Vankelecom, C. Vandecasteele, B. Van der Bruggen, Physico-chemical characterization of nanofiltration membranes, ChemPhysChem 8 (2007) 370–379.
[251] A. Al-Amoudi, Effect of chemical cleaning agents on virgin nanofiltration membrane as characterized by positron annihilation spectroscopy, Sep. Purif. Technol. 110 (2013) 51–56.
[252] T. Fujioka, N. Oshima, R. Suzuki, S.J. Khan, A. Roux, Y. Poussade, J.E. Drewes, L. D. Nghiem, Rejection of small and uncharged chemicals of emerging concern by reverse osmosis membranes: the role of free volume space within the active skin layer, Sep. Purif. Technol. 116 (2013) 426–432.
[253] D. Nanda, K.-L. Tung, W.-S. Hung, C.-H. Lo, Y.-C. Jean, K.-R. Lee, C.-C. Hu, J.-Y. Lai, Characterization of fouled nanofiltration membranes using positron annihilation spectroscopy, J. Membr. Sci. 382 (2011) 124–134.
[254] T. Shintani, A. Shimazu, S. Yahagi, H. Matsuyama, Characterization of methyl-substituted polyamides used for reverse osmosis membranes by positron annihilation lifetime spectroscopy and MD simulation, J. Appl. Polym. Sci. 113 (2009) 1757–1762.
[255] K.-S. Chang, Y.-H. Huang, K.-R. Lee, K.-L. Tung, Free volume and polymeric structure analyses of aromatic polyamide membranes: a molecular simulation and experimental study, J. Membr. Sci. 354 (2010) 93–100.
[256] A. Shimazu, K. Ikeda, T. Miyazaki, Y. Ito, Application of positron annihilation technique to reverse osmosis membrane materials, Radiat. Phys. Chem. 58 (2000) 555–561.
[257] J. Albo, H. Hagiwara, H. Yanagishita, K. Ito, T. Tsuru, Structural characterization of thin-film polyamide reverse osmosis membranes, Ind. Eng. Chem. Res. 53 (2014) 1442–1451.
[258] J. Lee, C.M. Doherty, A.J. Hill, S.E. Kentish, Water vapor sorption and free volume in the aromatic polyamide layer of reverse osmosis membranes, J. Membr. Sci. 425-426 (2013) 217–226.
[259] Z. Chen, K. Ito, H. Yanagishita, N. Oshima, R. Suzuki, Y. Kobayashi, Correlation study between free-volume holes and molecular separations of composite membranes for reverse osmosis processes by means of variable-energy positron annihilation techniques, J. Phys. Chem. C 115 (2011) 18055–18060.
[260] Y.C. Jean, W.-S. Hung, C.-H. Lo, H. Chen, G. Liu, L. Chakka, M.-L. Cheng, D. Nanda, K.-L. Tung, S.-H. Huang, K.-R. Lee, J.-Y. Lai, Y.-M. Sun, C.-C. Hu, C.-C. Yu, Applications of positron annihilation spectroscopy to polymeric membranes, Desalination 234 (2008) 89–98.
[261] A. Shimazu, H. Goto, T. Shintani, M. Hirose, R. Suzuki, Y. Kobayashi, Vacancy profile in reverse osmosis membranes studied by positron annihilation lifetime measurements and molecular dynamics simulations, J. Phys. Conf. Ser. 443 (2013), 012050.
[262] S.-H. Huang, W.-S. Hung, D.-J. Liaw, H.-A. Tsai, G.J. Jiang, K.-R. Lee, J.-Y. Lai, Positron annihilation study on thin-film composite pervaporation membranes: correlation between polyamide fine structure and different interfacial polymerization conditions, Polymer 51 (2010) 1370–1376.

[263] Y.-H. Huang, W.-C. Chao, W.-S. Hung, Q.-F. An, K.-S. Chang, S.-H. Huang, K.-L. Tung, K.-R. Lee, J.-Y. Lai, Investigation of fine-structure of polyamide thin-film composite membrane under swelling effect by positron annihilation lifetime spectroscopy and molecular dynamics simulation, J. Membr. Sci. 417-418 (2012) 201–209.
[264] H.H. Yin, Y. Zejie, M. Weitao, Z. Daming, A review of studies of polymeric membranes by positron annihilation lifetime spectroscopy, Plasma Sci. Technol. 7 (2005) 3062–3064.
[265] J. Li, B. Xiong, C. Yin, X. Zhang, Y. Zhou, Z. Wang, P. Fang, C. He, Free volume characteristics on water permeation and salt rejection of polyamide reverse osmosis membranes investigated by a pulsed slow positron beam, J. Mater. Sci. 53 (2018) 16132–16145.
[266] D.M. Davenport, C.L. Ritt, R. Verbeke, M. Dickmann, W. Egger, I.F.J. Vankelecom, M. Elimelech, Thin film composite membrane compaction in high-pressure reverse osmosis, J. Membr. Sci. 610 (2020) 118268.
[267] T. Fujioka, N. Oshima, R. Suzuki, W.E. Price, L.D. Nghiem, Probing the internal structure of reverse osmosis membranes by positron annihilation spectroscopy: gaining more insight into the transport of water and small solutes, J. Membr. Sci. 486 (2015) 106–118.
[268] M.M. Kłosowski, C.M. McGilvery, Y. Li, P. Abellan, Q. Ramasse, J.T. Cabral, A. G. Livingston, A.E. Porter, Micro-to nano-scale characterisation of polyamide structures of the SW30HR RO membrane using advanced electron microscopy and stain tracers, J. Membr. Sci. 520 (2016) 465–476.
[269] E.P. Chan, B.R. Frieberg, K. Ito, J. Tarver, M. Tyagi, W. Zhang, E.B. Coughlin, C. M. Stafford, A. Roy, S. Rosenberg, C.L. Soles, Insights into the water transport mechanism in polymeric membranes from neutron scattering, Macromolecules 53 (4) (2020) 1443–1450.
[270] T.E. Culp, Y.-x. Shen, M. Geitner, M. Paul, A. Roy, M.J. Behr, S. Rosenberg, J. Gu, M. Kumar, E.D. Gomez, Electron tomography reveals details of the internal microstructure of desalination membranes, Proc. Natl. Acad. Sci. 115 (2018) 8694–8699.
[271] J.-H. Lee, J.Y. Chung, E.P. Chan, C.M. Stafford, Correlating chlorine-induced changes in mechanical properties to performance in polyamide-based thin film composite membranes, J. Membr. Sci. 433 (2013) 72–79.
[272] J.Y. Chung, J.-H. Lee, K.L. Beers, C.M. Stafford, Stiffness, Strength, and Ductility of Nanoscale Thin Films and Membranes: A Combined Wrinkling–Cracking Methodology, Nano Letters, 11 (2011) 3361–3365.
[273] K.C. Khulbe, T. Matsuura, Thin Film Composite and/or Thin Film Nanocomposite Hollow Fiber Membrane for Water Treatment, Pervaporation, and Gas/Vapor Separation, Polymers, 10 (2018).
[274] M.I. Baig, P.G. Ingole, W.K. Choi, S.R. Park, E.C. Kang, H.K. Lee, Water vapor permeation behavior of interfacially polymerized polyamide thin film on hollow fiber membrane substrate, J. Taiwan Inst. Chem. Eng. 60 (2016) 623–635.
[275] P.G. Ingole, W.K. Choi, G.B. Lee, H.K. Lee, Thin-film-composite hollow-fiber membranes for water vapor separation, Desalination 403 (2017) 12–23.
[276] J. Zuo, Y. Wang, S.P. Sun, T.-S. Chung, Molecular design of thin film composite (TFC) hollow fiber membranes for isopropanol dehydration via pervaporation, J. Membr. Sci. 405-406 (2012) 123–133.
[277] P. Sukitpaneenit, T.-S. Chung, Fabrication and use of hollow fiber thin film composite membranes for ethanol dehydration, J. Membr. Sci. 450 (2014) 124–137.
[278] Y. Zhang, N.L. Le, T.-S. Chung, Y. Wang, Thin-film composite membranes with modified polyvinylidene fluoride substrate for ethanol dehydration via pervaporation, Chem. Eng. Sci. 118 (2014) 173–183.
[279] P.G. Ingole, W. Choi, K.-H. Kim, H.-D. Jo, W.-K. Choi, J.-S. Park, H.-K. Lee, Preparation, characterization and performance evaluations of thin film composite hollow fiber membrane for energy generation, Desalination 345 (2014) 136–145.
[280] G. Han, T.-S. Chung, Robust and high performance pressure retarded osmosis hollow fiber membranes for osmotic power generation, AICHE J. 60 (2014) 1107–1119.
[281] S. Chou, L. Shi, R. Wang, C.Y. Tang, C. Qiu, A.G. Fane, Characteristics and potential applications of a novel forward osmosis hollow fiber membrane, Desalination 261 (2010) 365–372.
[282] Y. Chen, L. Setiawan, S. Chou, X. Hu, R. Wang, Identification of safe and stable operation conditions for pressure retarded osmosis with high performance hollow fiber membrane, J. Membr. Sci. 503 (2016) 90–100.
[283] S. Chou, R. Wang, L. Shi, Q. She, C. Tang, A.G. Fane, Thin-film composite hollow fiber membranes for pressure retarded osmosis (PRO) process with high power density, J. Membr. Sci. 389 (2012) 25–33.
[284] C.F. Wan, T. Yang, W. Gai, Y.D. Lee, T.-S. Chung, Thin-film composite hollow fiber membrane with inorganic salt additives for high mechanical strength and high power density for pressure-retarded osmosis, J. Membr. Sci. 555 (2018) 388–397.
[285] S. Lim, V.H. Tran, N. Akther, S. Phuntsho, H.K. Shon, Defect-free outer-selective hollow fiber thin-film composite membranes for forward osmosis applications, J. Membr. Sci. 586 (2019) 281–291.
[286] W. Gai, D.L. Zhao, T.-S. Chung, Thin film nanocomposite hollow fiber membranes comprising Na+-functionalized carbon quantum dots for brackish water desalination, Water Res. 154 (2019) 54–61.
[287] M. Mondal, S. De, Treatment of textile plant effluent by hollow fiber nanofiltration membrane and multi-component steady state modeling, Chem. Eng. J. 285 (2016) 304–318.
[288] S. Jana, A. Mondal, A. Ghosh, Fabrication of stable NiO/Fe2O3 heterostructure: a versatile hybrid material for electrochemical sensing of glucose, methanol and enhanced photodecomposition and/photoreduction of water contaminants, Appl. Catal. B Environ. 232 (2018) 26–36.
[289] M. Mohammadifakhr, K. Trzaskus, A.J.B. Kemperman, H.D.W. Roesink, J. de Grooth, Increasing the success rate of interfacial polymerization on hollow fibers by the single-step addition of an intermediate layer, Desalination 491 (2020) 114581.
[290] Y. Yabuno, K. Mihara, K. Komatsu, S. Shimamura, K. Nakagawa, T. Shintani, H. Matsuyama, T. Yoshioka, Preparation of polyamide thin-film composite membranes using hydrophilic hollow fiber PVDF via the TIPS process modified by PVA diffusion, Ind. Eng. Chem. Res. 58 (2019) 21691–21699.
[291] Y. Lin, Y. Chen, R. Wang, Thin film nanocomposite hollow fiber membranes incorporated with surface functionalized HKUST-1 for highly-efficient reverses osmosis desalination process, J. Membr. Sci. 589 (2019) 117249.
[292] Y. Zhang, L. Yang, K.P. Pramoda, W. Gai, S. Zhang, Highly permeable and fouling-resistant hollow fiber membranes for reverse osmosis, Chem. Eng. Sci. 207 (2019) 903–910.
[293] S. Veríssimo, K.V. Peinemann, J. Bordado, Thin-film composite hollow fiber membranes: An optimized manufacturing method, J. Membr. Sci. 264 (2005) 48–55.

Supporting Information

A Review on the Synthesis of Fully Aromatic Polyamide Reverse Osmosis Membranes

Shahriar Habib and Steven T. Weinman*

Department of Chemical and Biological Engineering, The University of Alabama, Tuscaloosa, AL 35487, USA

*Corresponding author: Tel: +1 (205)-348-8516, Fax: +1 (205)-348-7558. Email address: stweinman@eng.ua.edu

Outliers

Outliers were removed from the data in Figures 6 and 9 from the main manuscript. Lower outliers were determined as values which were lower than quartile 1 (Q1) minus 1.5 times the inter-quartile range (IQR) (Q1 – 1.5*IQR). Upper outliers were determined as values which were greater than quartile 3 (Q3) plus 1.5 times the IQR (Q3 + 1.5*IQR).

Statistical Analysis

Hypothesis testing for the mean results from Figures 6 and 9 from the main manuscript was done to determine the statistical relevance of the data sets. The Analysis ToolPak of Microsoft Excel for Office 365 was used for all statistical analyses. Interpretation (what is statistically different) of a multiple mean hypothesis test was done using an Analysis of Variance (ANOVA). A post-hoc test with the Bonferroni correction was used when at least two means were statistically different in the ANOVA test. ANOVA tests were done using 95% confidence ($\alpha = 0.05$); therefore, if the p-value is greater than α then all the means are considered to be statistically the same and if

the p-value is less than α then at least two of the means are considered to be statistically different. When doing a post-hoc test, a Bonferroni correction was used. The Bonferroni correction is done by dividing α = 0.05 by the number of means used in the analysis. For the post-hoc test, if the p-value was greater than α then the means are considered to be statistically the same and if the p-value was less than α then the means are considered to be statistically different.

The effect of aqueous MPD solution soaking time on the water permeance data from Figure 6A in the main manuscript was analyzed using an ANOVA test. **Table S1** shows the results for the statistical analysis for MPD soaking times of 1 (n = 6) 2 (n = 15), and 5 (n = 9) min. At least two of the average water permeances were found to be statistically different. A post-hoc test with a Bonferroni correction was done where an α = 0.05/3 = 0.0167 was used. According to the post-hoc analysis, the water permeance of the 1 min and 5 min MPD soaked membranes was statistically different. The water permeance of the 1 and 2 min and the 2 and 5 min MPD soaked membranes were found to be statistically the same.

Table S1. Statistical analysis results of the water permeance of 1 min, 2 min, and 5 min aqueous MPD solution soaked membranes.

Test Variable	Test	Equal Means p-value	Interpretation (95% Confidence)
Water permeance of 1 min, 2 min, and 5 min	ANOVA	0.00106	Statistically different
Water permeance of 1 min and 2 min	Post-hoc test with Bonferroni correction	0.02130	Statistically the same
Water permeance of 1 min and 5 min	Post-hoc test with Bonferroni correction	0.00009	Statistically different
Water permeance of 2 min and 5 min	Post-hoc test with Bonferroni correction	0.05839	Statistically the same

The effect of aqueous MPD solution soaking time on the NaCl rejection data from Figure 6B in the main manuscript was analyzed using an ANOVA test. **Table S2** shows the results for the statistical analysis for MPD soaking times of 1 (n = 5) 2 (n = 15), and 5 (n = 10) min. At least two of the average NaCl rejections were found to be statistically different. A post-hoc test with a Bonferroni correction was done where an $\alpha = 0.05/3 = 0.0167$ was used. According to the post-hoc analysis, the NaCl rejection of the 2 min and 5 min MPD soaked membranes was statistically different. The NaCl rejection of the 1 min and 2 min and the 1 min and the 5 min MPD soaked membranes were found to be statistically the same.

Table S2. Statistical analysis results of the NaCl rejection of 1 min, 2 min, and 5 min aqueous MPD solution soaked membranes.

Test Variable	Test	Equal Means p-value	Interpretation (95% Confidence)
NaCl rejection of 1 min, 2 min, and 5 min	ANOVA	0.00400	Statistically different
NaCl rejection of 1 min and 2 min	Post-hoc test with Bonferreni correction	0.08687	Statistically the same
NaCl rejection of 1 min and 5 min	Post-hoc test with Bonferreni correction	0.17358	Statistically the same
NaCl rejection of 2 min and 5 min	Post-hoc test with Bonferreni correction	0.00306	Statistically different

The effect of different organic co-solvents used during interfacial polymerization on the water permeance data from Figure 9A in the main manuscript was analyzed using an ANOVA test. **Table S3** shows the results for the statistical analysis of the water permeance of membranes made with no co-solvent (n = 18) and Ethyl Acetate (n = 13), Diethyl Ether (n = 13), and Acetone (n = 7) as co-solvents in the organic solvent during interfacial polymerization. At least 2 of the average water permeances were found to be statistically different. A post-hoc test with a Bonferroni

correction was done where an $\alpha = 0.05/4 = 0.0125$ was used. According to the post-hoc analysis, the water permeance of the no co-solvent membranes were statistically different than the Ethyl Acetate, Diethyl Ether, and Acetone organic co-solvent membranes. The water permeance of Ethyl Acetate and Diethyl Ether, Ethyl Acetate and Acetone, and Diethyl Ether and Acetone organic co-solvent membranes were found to be statistically the same.

Table S3. Statistical analysis results of the water permeance of membranes made with no co-solvent and Ethyl Acetate, Diethyl Ether, and Acetone as co-solvents in the organic solvent during interfacial polymerization.

Test Variable	Test	Equal Means p-value	Interpretation (95% Confidence)
Water permeance of No Co-Solvent, Ethyl Acetate, Diethyl Ether, and Acetone	ANOVA	0.00003	Statistically different
Water permeance of No Co-Solvent and Ethyl Acetate	Post-hoc test with Bonferreni correction	0.00146	Statistically different
Water permeance of No Co-Solvent and Diethyl Ether	Post-hoc test with Bonferreni correction	0.00111	Statistically different
Water permeance of No Co-Solvent and Acetone	Post-hoc test with Bonferreni correction	0.00175	Statistically different
Water permeance of Ethyl Acetate and Diethyl Ether	Post-hoc test with Bonferreni correction	0.67868	Statistically the same
Water permeance of Ethyl Acetate and Acetone	Post-hoc test with Bonferreni correction	0.08384	Statistically the same
Water permeance of Diethyl Ether and Acetone	Post-hoc test with Bonferreni correction	0.24067	Statistically the same

The effect of different organic co-solvents used during interfacial polymerization on the NaCl rejection data from Figure 9B in the main manuscript was analyzed using an ANOVA test. **Table S4** shows the results for the statistical analysis for of the NaCl rejection of membranes made with no co-solvent (n = 18) and Ethyl Acetate (n = 13), Diethyl Ether (n = 11), and Acetone (n = 7) as co-solvents in the organic solvent during interfacial polymerization. The average NaCl

rejections were found not to be statistically different, therefore the post-hoc analysis was not required.

Table S4. Statistical analysis results of the NaCl rejection of membranes made with no co-solvent and Ethyl Acetate, Diethyl Ether and Acetone as co-solvents in the organic phase during interfacial polymerization.

Test Variable	Test	Equal Means p-value	Interpretation (95% Confidence)
NaCl rejection of No Co-Solvent, Ethyl Acetate, Diethyl Ether, and Acetone	ANOVA	0.13724	Statistically the same